Journal of Manufacturing Processes 54 (2020) 393–412

Contents lists available at ScienceDirect

Journal of Manufacturing Processes

journal homepage: www.elsevier.com/locate/manpro

Investigate on computer-aided fixture design and evaluation algorithm for near-net-shaped jet engine blade

Dongbo Wu[a], Bing Zhao[a,b], Hui Wang[a,*], Kaiyao Zhang[a,c], Jie Yu[d]

[a] State Key Laboratory of Tribology, Beijing Key Lab of Precision/Ultra-Precision Manufacturing Equipment and Control, Department of Mechanical Engineering, Tsinghua University, Beijing, 100084, PR China
[b] Department of Mechanical Engineering, Qinghai University, Xining, 810016, PR China
[c] Yantai University. Yantai, Shandong, 264005, PR China
[d] AECC Xi'an Aero-engine LTD, Xi'an, Shannxi, 710021, PR China

ARTICLE INFO

Keywords:
Computer-aided technology
Fixture design and evaluation
Positioning error transmission model
Near-net-shaped jet engine blade

ABSTRACT

This study proposes a computerized framework for computer-aided fixture design and evaluation for near-net-shaped jet engine blades. First, the manufacturing process of near-net-shaped jet engine blades and requirements for the fixture design and evaluation were analyzed. Second, a numerical model of the positioning error and the corresponding experimental platform were established. Third, a mechanical model of the blade under cutting conditions was analyzed, a finite element model (FEM) was established. Fourth, a mathematical model of the machining fixture layout optimization was established, and the positioning clamping points of the machining fixture were optimized by the combination of finite element analysis (FEA) and genetic algorithm. Finally, the corresponding algorithm verification was carried out by positioning error and cutting experiments. The results showed that the proposed computerized framework could evaluate and optimize the fixture of the same type blade to obtain the positioning and mechanical behavior of the fixture, and can realize high-precision manufacturing of near-net-shaped jet engine blades.

1. Introduction

Blades, especially rotor blades, are one of the most critical components in jet engines, and their quality has a great impact on the performance and service life of the jet engine.

Blades working environments are relatively harsh, and they must run at high speeds, exceeding 10,000 rpm (RPM) and bear huge centrifugal forces and air resistance [1]. The large number of blades, complex shapes, and high-performance demands create strict requirements for the advanced manufacturing processes of jet engine blades, such as the blade materials, machining process, heat treatment, and surface spraying process [2].

To achieve a high performance and low weight, the material of the jet engine blade is generally a titanium or high-temperature alloy, and these materials are typically difficult to machine materials [3]. To achieve an excellent aerodynamic performance and the maximum thrust ratio, the jet engine blade is a complex curved structure that is designed based on aerodynamic experiments. The blade thickness is generally small, typically 2–5 mm. The radius of the blade leading and trailing edge (LTE) is very small, typically about 1–2 mm. The curvature of the blade surface varies tremendously from a point to another point on the blade surface. Due to these structural and material characteristics, the manufacturing accuracy control and performance improvement of blades are exceedingly important [4]. Precision CNC machining, as the last step in blade fabrication, is a key process to improve the manufacturing accuracy and performance of the blade and the performance of the jet engine.

Near-net-shaped processes, such as the precision forging process, is a typical additive manufacturing technology, and this process can reduce the material waste and improve the service performance [5]. In this process, the blade profile is guaranteed by precision forging, and the forming accuracy is sufficiently high to fully meet the accuracy requirements of the blade. Therefore, the maximum area of the blade (body part) will no longer require subsequent CNC machining. However, the blade tenon root, LTE and tip cannot be formed by the precision forging process and must be CNC machined due to the precision forging process cannot ensure the manufacturing accuracy of small curvature components.

Machining fixture is a guarantee of the accuracy the CNC machining during the CNC machining process of the blade tenon root and tip

* Corresponding author.
E-mail address: wanghuisx@gmail.com (H. Wang).

https://doi.org/10.1016/j.jmapro.2020.02.023
Received 7 October 2019; Received in revised form 21 January 2020; Accepted 18 February 2020

[6–8]. In particular, the positioning and clamping scheme is more important and critical. Unfortunately, machining fixture design faces greater challenges in the machining of precision forged blades due to the positioning and clamping points are only on the blade body surface, which is a typical thin-walled free-surface part with a low stiffness [9]. Therefore, the design and evaluation of the fixture are necessary and important.

At present, a low-melting alloy casting process is used as the machining fixture for CNC machining of precision forging blade tenon root, and this will lead to the pollution and poor efficiency [10,11]. Therefore, the scheme of multi-point direct positioning and clamping is a good choice for the current blade CNC machining process along with the manufacturing of blades is transitioning to intelligent manufacturing.

There have been many studies on the analysis of the performance analysis method of fixture, especially focused on the mechanical behavior and the positioning performance of the fixture. Estrems et al. [12] proposed that a workpiece size variable function based on the accuracy should be firstly established, after which the positioning location and the error transmission of the size chain of the fixture and parts should be analyzed. The actual value of the key size and potential imprecision (deviation) should finally be determined. Rong et al. [13] comprehensively studied and described the effect of the positioning error on the precision of the workpiece machining, and established a complete geometric error calculation and sensitivity factor analysis method. Wang et al. [14,15] studied the influence of the positioning error on the machining error based on the fixture and contour errors of the workpiece. They integrated the CNC machining path with the fixture design and finally optimized the structure and layout of the fixture by geometric interference path simulation planning. Katz et al. [16] proposed the concept of "closed-loop machining cells," which was an integrated method of blade processing involving "installation– detection– machining optimization," and the Newton–Raphson technique was used to develop a mathematical model that predicted the impact of fixture locating points on the workpiece accuracy.

Many scholars have conducted research on the optimization design of thin-walled part fixtures. Gene et al. proposed a dynamic model and analysis method for a workpiece–fixture system, and analyzed the influence of the fixture size, position, and sequence on the fixture [17]. Hamedi et al. studied a nonlinear FEA system combining an artificial neural network and genetic algorithm, and analyzed the optimal clamping force of the fixture [18]. Wang et al. optimized the clamping deformation of thin-walled curved parts by FEA [19]. Qin et al. established a mathematical model to analyze the influence of the clamping force and clamping sequence on the deformation [20]. Zhou et al. optimize the fixture layout and clamping force of the fixture by genetic algorithm [21,22].

Based on the above analyses, the previous studies focused on optimizing fixture by FEA and genetic algorithms, and this method is reasonable and feasible. Due to the special characteristics of precision forged blades (near-net-shaped jet engine blades) which mainly reflects in the blade structure, the clamping scheme and CNC machining process, it is urgent to combine geometric analysis, FEA and algorithm analysis to summarized as a computer-aided fixture design and evaluation method, that is, to establish a computer aided design and evaluation method for the CNC machining fixture of precision forged blades for the special structures and manufacturing processes. Therefore, this paper mainly focuses on the fixture design and evaluation method by computer-aided technology. In Section 2, a technical framework for the computer–aided fixture design and evaluation is introduced. In Section 3, the algorithms and models of the computer-aided fixture design and evaluation are introduced. First, the mathematical model of the fixture positioning error transmission is established, and the mechanism of the fixture positioning error transmission is obtained. Second, the FEM for the blade–fixture system was established, and the mechanical behavior of the blade–fixture system was analyzed by micron -scale manufacturing error mechanical model to explain the impact of non-ideal fixture manufacturing errors on the fixture system mechanical behavior. Third, a computer-aided fixture layout optimization method is established by FEA and genetic algorithm. The corresponding experimental platforms are introduced in Section 4. The simulation and experimental results are analyzed and discussed in Section 5. Finally, results are summarized and discussed in Section 6.

2. Fixture design and evaluation of blades

In a jet engine, the rotor is mainly composed of shaft components and an impeller which mainly includes a blade and blisk, and it can be further divided into high- and low-pressure rotors. The stator is mainly composed of a stator blade, bearing frame, and casing. The blade is the most used functional part in the jet engine and is a key component for ensuring the engine performance. Generally, there are about 3000 types of rotor and stator blades in a jet engine, and it is the most important component for achieving the function of the jet engine. The manufacturing accuracy and performance of the blade has a big impact on the service performance and life of a jet engine.

Fig. 1 shows a typical near-net-shaped blades. The blade body part does not require secondary CNC machining, that is, it is formed by a precision forging process. However, the tenon root, tip and the LTE of the blade require subsequent CNC machining due to the poor accuracy and process characteristics of the precision forging process. The material must be removed from the tenon root and tip of the blade. Only the blade body can be used as the positioning and clamping surface during the CNC machining of the tenon root and tip of the blade, which creates difficulties for the fixture design and evaluation. Thus, positioning analysis, fixture mechanical properties analysis, and clamping layout optimization in the fixture design will be difficult during blade production.

More importantly, it will be very inefficient to be carried out the design and evaluation of the fixture for each blade because there are so many types and numbers of blades in a jet engine. Therefore, it is necessary to develop a general-purpose software of the computer-aided fixture design and evaluation to achieve the design and evaluation of fixture of same type blade, and form a systematic fixture design and evaluation method, which is necessary for the manufacture of the blade.

Fig. 2 shows the technical framework for the fixture design and evaluation. First, the positioning performance of the fixture should be evaluated by computer-aided technology, which mainly models the geometric relationships. The geometric model of the positioning error transmission of the thin-walled complex curved surface blade should be established to obtain the mapping relationship of the positioning error and the fixture, and to achieve the transmission relationship of the positioning error from the fixture to the tenon root of blade. Second, the

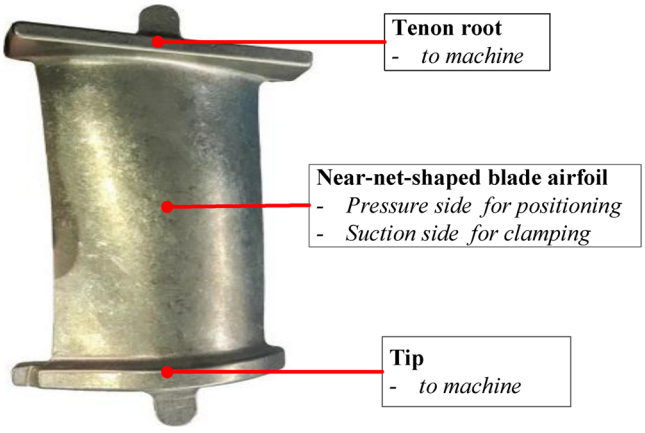

Fig. 1. Typical titanium alloy near-net-shaped jet engine blades.

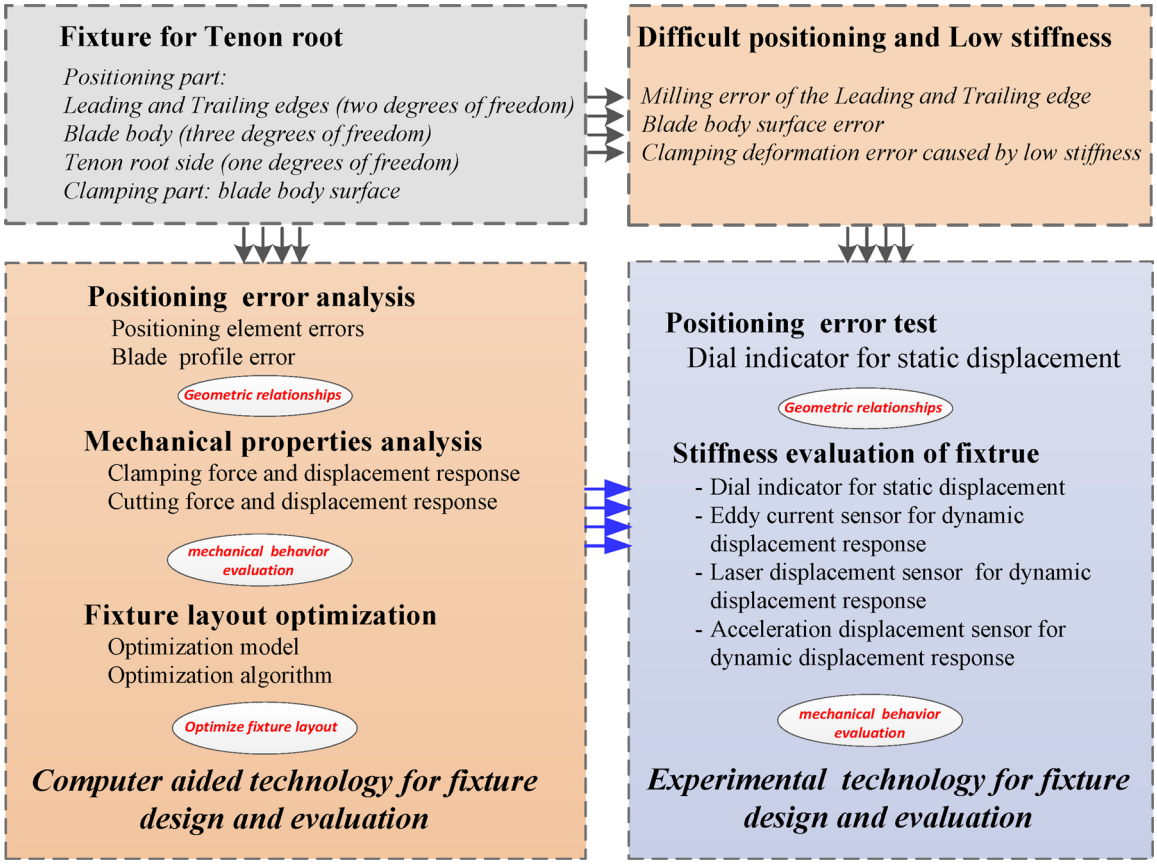

Fig. 2. Technical framework for fixture design and evaluation.

mechanical properties of the blade–fixture system was analyzed and evaluated, which is mainly to establish a FEM to evaluate the ability of the fixture to carry cutting and clamping forces which can reflect the stiffness of the fixture. Finally, the fixture layout optimization model was established based on the established FEM and genetic algorithm. These three models, that is, the positioning error transfer model, the FEM of the blade–fixture system and the optimization model of the blade–fixture layout, constitute a computer-aided technical system for the fixture design and evaluation of a blade.

In actual CNC machining processes, the concept of flexible production is necessary because there are so many blades in a jet engine, and thus, it is impossible to construct a corresponding production line for each blade. Therefore, the fixture design also must adopt a creative design concept to realize flexible manufacturing in a stationary production line, and the new fixture should be adapted to this production line to improve the processing efficiency. In this study, the third-stage stator compressor blade was taken as an example, and its containment boundary was 220 × 100 × 5 mm, and the corresponding algorithm and model were analyzed based on this blade. In addition, the first-stage rotor blade of the same jet engine with a containment boundary of 100 × 50 × 4 mm was used as the test blade to verify the feasibility of this computer aided method of fixture design and evaluation. This is, the above-mentioned algorithms and models were used to design the corresponding fixture and were matched to the same production line to achieve high efficiency and high-performance manufacturing of this blade.

3. Analysis of principles and methods of fixture computer-aided technology

3.1. Modeling of positioning geometry of the blade– fixture system

In the blade clamping process, the thin-walled curved surface, as a positioning reference, has a contour error in the precision forging process. Meanwhile, the positioning element on the blade clamping device also has a manufacturing error certain error. Therefore, the actual positioning point will deviate from the theoretical position. Moreover, a small displacement of the position will lead to a large change of the blade's overall position because the positioning surface is a freeform curved surface with a certain curvature. Therefore, the tenon root will deviate from the theoretical position before CNC machining and cause large processing distortions.

First, the positioning deviation of the positioning element on the fixture can be expressed as follows:

$$\delta_{fL}(i) = [\Delta x, \Delta y, \Delta z]^T \quad i = 1, 2, \cdots, 6 \tag{3.1}$$

where Δx is the deviation of the positioning element in the x- axis direction, Δy is the deviation of the positioning element in the y- axis direction, Δz is the deviation of the positioning element in the z- axis direction, specifically refers to the position deviation between the theoretical model of the positioning element and the actual value, and the bottom surface of the positioning element in the theoretical model is a reference. $\delta_{fL}(i)$ is the position change of the observation point on the blade, and the corresponding observation point on the theoretical model of the blade is the reference point.

Second, there was a contour error in the blade profile, which was used as a position reference, and the contour error tolerance is T_0. In fact, contour error is the error of the blade profile surface after precision forging process (near-net-shaped jet engine blades), and this error is the manufacturing error of the precision forging process (near-net-shaped jet engine blades), the exist of this contour error is mainly due to insufficient manufacturing capacity of the precision forging process, however, this error value satisfies the requirements of blade manufacturing accuracy. There is a long time of production experience in Xi'an Aero-Engine (Group) Ltd, Xi'an, which shows that the contour

error is about 0.005 mm-0.08 mm. The researched blade was a high-precision formed part, and the magnitudes of the position and shape errors were very small relative to their own structural dimensions, which can be expressed as follows:

$$\delta_i/N_i \to 0 \tag{3.2}$$

where δ_i represents the position and contour errors, and N_i represents the structural dimensions of the blade.

The actual positioning point of the blade also changes slightly in the neighborhood of its nominal positioning point under the influence of geometric errors. Therefore, it was assumed that the blade and fixture maintained stable contact with each other even if the error existing of the fixture and the blade to simplify the analysis problem, which can be expressed as follows:

$$P_{fL}(i) = P_{sL}(i) \quad i = 1, 2, \cdots, 6 \tag{3.3}$$

All the points of the blade were changed in the same way, since the spatial positional relationship between any two points on the blade was fixed. The position change process from a certain point P to P^* is regarded as a combined transformation of the rotation and translation processes. The rotation vector is $\mathbf{R}$ and the translation vector is $\mathbf{T}$, which can be expressed as follows:

$$\mathbf{P}^*(x, y, z) = \mathbf{R} \times \mathbf{P}(x, y, z) + \mathbf{T} \tag{3.4}$$

There are six variables in the spatial variation of the blades, three rotations and three translations. If the six variables and the original position of the blade are known, the overall position and posture of the blade after the change can be obtained. Therefore, it is important to solve the blade space change matrix.

The blade positioning error was a combination of the blade contour error and positioning element error. The change in position and posture caused by the positioning error can be approximated using Eq. (3.4). Thus, the actual position change of the tenon root can be specifically solved using Eqs. (3.2) and (3.3). The Rodriguez matrix is used to solve the spatial variation matrix [R, **T**] of the blade, and the anti-symmetric matrix is obtained:

$$\mathbf{S} = \begin{bmatrix} 0, -c, -b \\ c, 0, -a \\ b, a, 0 \end{bmatrix} \tag{3.5}$$

The Rodriguez rotation matrix is obtained as follows:

$$R = (I + S)(I - S)^{-1} \tag{3.6}$$

From Eqs. (3.5) and (3.6), the following equation can be obtained:

$$\mathbf{R} = \frac{1}{1 + a^2 + b^2 + c^2} \begin{bmatrix} 1 + a^2 - b^2 - c^2, -2ab - 2c, -2b + 2ac \\ 2c - 2ab, 1 - a^2 + b^2 - c^2, -2a - 2bc \\ 2ac + 2b, 2a - 2bc, 1 - a^2 - b^2 + c^2 \end{bmatrix} \tag{3.7}$$

The translation matrix is defined as follows:

$$\mathbf{T} = [T_x, T_y, T_z] \tag{3.8}$$

If the deviations of the six positioning points are known, substituting Eq. (3.4) yields the following:

$$P^*_{sL}(i) = P_{sL}(i) + \delta_{sL}(i) = R \times P_{sL}(i) + T \quad i = 1, 2, \cdots, 6 \tag{3.9}$$

First, Equations (3.3–3.9) can be used to establish a system of 18 equations, in which the undetermined parameters are $[a, b, c, T_x, T_y, T_z]$. Second, the least squares method can be used to determine these parameters to obtain the approximate solution of the spatial variation matrix [R, **T**] of the blade. Finally, the position change of the tenon root due to the positioning error can be obtained.

3.2. FEM of blade–fixture system

During the CNC machining of the blade tenon root, the blade tenon root is affected by the cutting and clamping forces, and the cutting force is a dynamically varying force over time and space during the actual machining process. Therefore, according to classical mechanic theory, the dynamic equation can be described as the dynamical deformation during the CNC machining process caused by the cutting force, as follows:

$$[M](\ddot{d}) + [C](\dot{d}) + [K]\{d\} = \{F_{(t)}\} \tag{3.10}$$

To facilitate the solution of the model, the dynamic process is transformed into a static process under the model assumption. Thus, the influence of inertia and damping on the blade–fixture system is not considered, and the stiffness matrix is continuous. Therefore, Eq. (3.10) can be converted to a linear static structure, as follows:

$$[K]\{d\} = \{F_{(t)}\} \tag{3.11}$$

However, a blade is a complex thin-walled part of a free-form surface, and its shape function is uncertain. Thus, it is difficult to obtain an analytical solution. Using computer-aided technology, the FEA is one of the most effective methods for solving this problem.

A FEM was established based on specific structural and mechanical characteristics:

(1) The simplified blade–fixture system was meshed, and there were 21,700 nodes and 10,070 units.
(2) The boundary conditions of the FEM are very important for obtaining an accurate solution. First, there were 8 elastically constrained contact faces between the simplified blade and the fixture component, wherein $\boldsymbol{P_i}$ (i = 1–4) was in frictional contact with the blade, and the friction coefficient μ = 0.48. $\boldsymbol{Q_j}$ (j = 1–4) contacted the blade and was defined as bonded contact. Finally, the load condition was given, and the bottom end of the four positioning heads $\boldsymbol{Q_j}$ (j = 1–4) did not produce displacement. The four clamping heads, $\boldsymbol{P_i}$ (i = 1–4), were clamped by 2200 N of pressure force, and a cutting force of 8 N, which was used to simulate external loads, acted perpendicularly at the end of the blade tenon root.
(3) Finite element solver was used to obtain the blade deformation.

To facilitate the final problem solving, it was necessary to make additional assumptions:

(1) During the processing of the blade tenon root, the blade will be elastically deformed in the longitudinal direction due to the cutting load under the clamping condition, and the model can be simplified as eight cylinders to clamp the blade. The simplified model is shown in Fig. 3.
(2) The contact areas of the four clamping points are the same, and the four clamping forces are the same.
(3) The blade tenon root is subjected to a time-varying cutting load during the actual machining process. However, the blade deformation is greatest when the cutting force acts on the ends of the blade tenon root. Therefore, it is assumed that a static load is applied to the far right of blade tenon root in this model [21].

3.3. Modeling of fixture layout optimization

In the CNC machining process of the precision forging blade tenon root, the new fixture mainly uses multi-point positioning and direct clamping scheme to clamp the blade body [9]. The precision forged blade, as a typical near-net-shaped blade, is a thin-walled freeform curved surface. Its material is a titanium alloy (elastic modulus 110 GPa), and the material of the positioning and clamping heads are

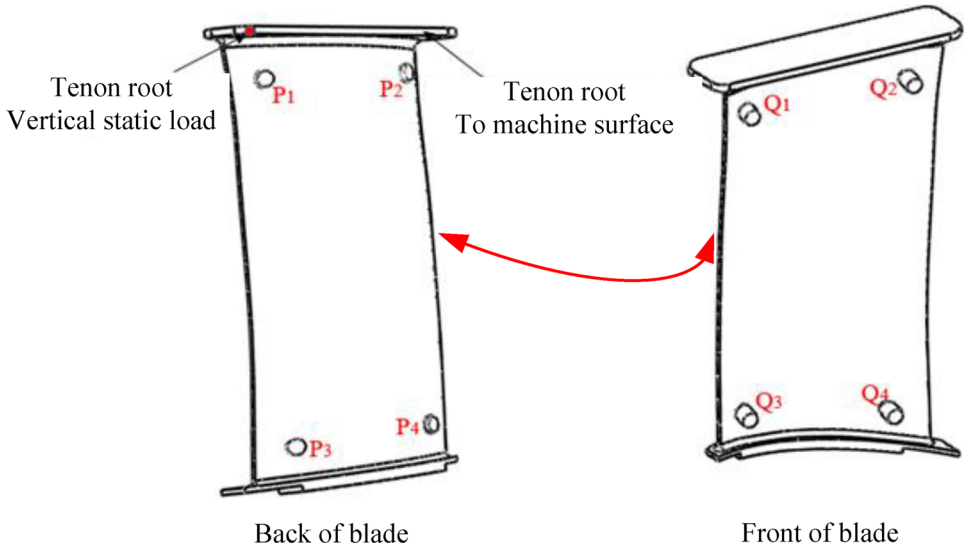

Fig. 3. Simplified model of blade clamping scheme, only considering the deformation in the *z*-direction.

PEEK-GF30 (elastic modulus 7 GPa).

The clamping mechanism of the new fixture consists of four clamping points, five positioning points, and four auxiliary positioning points, as shown in Fig. 4. During the CNC machining process of the blade tenon root, the fixture mainly clamps the blade body by four clamping points at the back of the blade. The initial four clamping points on the blade surface based on the blade precision forging coordinate system are empirically selected by designers. However, in the actual blade CNC machining process, the position layout of the four clamping points is determined by the blade–fixture system stiffness. The initial four clamping points must be iterated based on the system stiffness using the computer-aided technology. Therefore, rationally arranging the positions of the four clamping points of the new fixture can effectively improve the stiffness of the blade-fixture system, thereby improving the processing quality of the blade tenon root. This requires computer-aided fixture design instead of traditional fixture design based on experience.

To determine the optimal position of the fixture layout, the layout of each clamping position within the blade containment boundary is optimized (the initial position of the blade clamping point is shown as $\boldsymbol{P_1}$, $\boldsymbol{P_2}$, $\boldsymbol{P_3}$, and $\boldsymbol{P_4}$ in Fig. 4(a), which is based on the reference coordinate system for the precision forging process, and the positions of the clamping points are summarized in Table 1.

The minimum value of the maximum deformation of the blade tenon root is selected as the objective function, expressed as follows:

$$dmax = \min(\max(|d_1|, |d_2|, \ldots, |d_k|, \ldots, |d_n|)) \tag{3.12}$$

where $dmax$ represents the optimal deformation amount, d_i represents the deformation amount of the blade during the machining process, and n represents the number of selected samples. A larger n indicates that it is closer to actual working conditions.

The position point range changes are shown as follows:

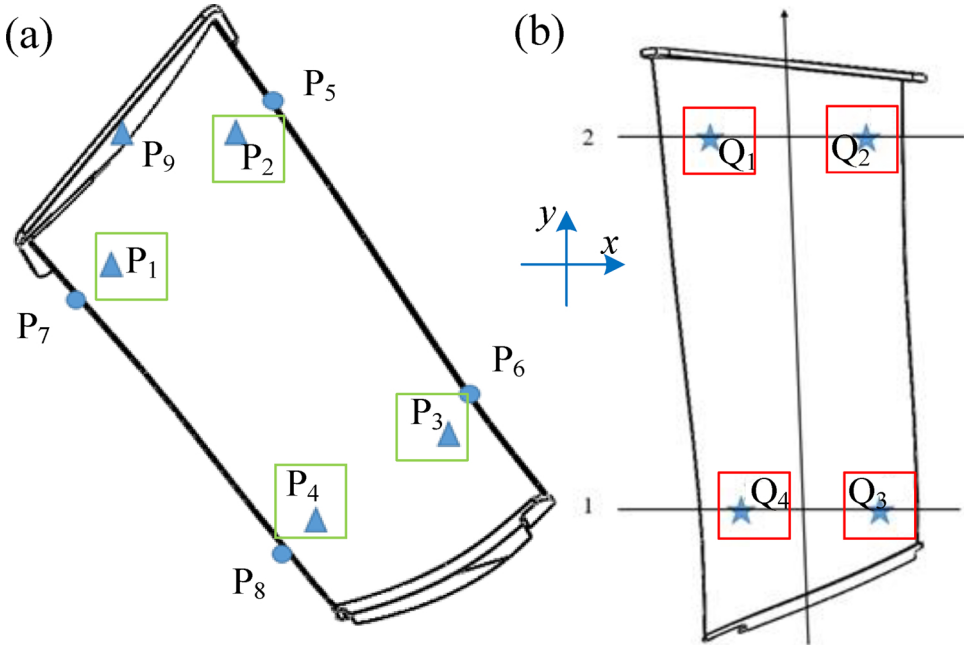

Fig. 4. Positioning and clamping layout of fixture: (a) multi-point positioning scheme for blade and (b) optimized range of clamping points.

Table 1
Blade body clamping point position.

Clamping point	P_1	P_2	P_3	P_4
Position	x_1, y_1	x_2, y_2	x_3, y_3	x_4, y_4

$$\left.\begin{array}{l} 24.2 \le x_1 \le 29.7,\ 2.5 \le y_1 \le 3.1 \\ 26 \le x_2 \le 31.8,\ 1.3 \le y_2 \le 1.6 \\ 21.3 \le x_3 \le 26,\ 103.7 \le y_3 \le 126.7 \\ 21.3 \le x_4 \le 26,\ 100.1 \le y_4 \le 122.3 \end{array}\right\} \quad (3.13)$$

The cutting force load is as follows:

$$t\,|F_{ti}| \ge \sqrt{F_{xi}^2 + F_{yi}^2}\ i = 1,\ 2,\ 3,\ 4 \quad (3.14)$$

where F_{ti} is the required clamping force for stable clamping, F_{xi} and F_{yi} are the tangential forces between the clamping element and blade body, and t is the friction factor.

The genetic algorithm is a randomized search method that simulates the survival of the fittest. The genetic algorithm can be used to determine the clamping component layout of the blade–fixture. The position of the clamping component must be randomly reorganized within the containment boundary to obtain multiple sets of solutions combined with the FEM. Finally, the best blade–fixture layout was obtained, and the flow chart for determining the optimal layout scheme of the blade–fixture is shown in Fig. 5.

In traditional genetic algorithms, roulette is used to select the appropriate chromosome. However, the selection ability is insufficient, and it is prone to obtain the local convergence and ignore the global optimal solution. The Pareto advantage is suitable for obtaining the accurate global optimal solutions, and it can be well combined with the finite element calculation tools (ANSYS) based on secondary development. Therefore, roulette was replaced with the Pareto advantage in this study. In particular, the Pareto advantage provides a set of solutions by sacrificing at least one target or constraint group to improve the other target or constraint when the goals and constraints conflict with each other.

For the multi-objective optimization, it is assumed that there is a set X that satisfies the constraints, and the problem of optimization of all feasible solutions can be simplified as $\min \overrightarrow{f(x)},\ x \in X$. If $x' \in X$, then all the objective functions are optimal. However, in reality, it is impossible for the all the cases to achieve optimal values at the same point.

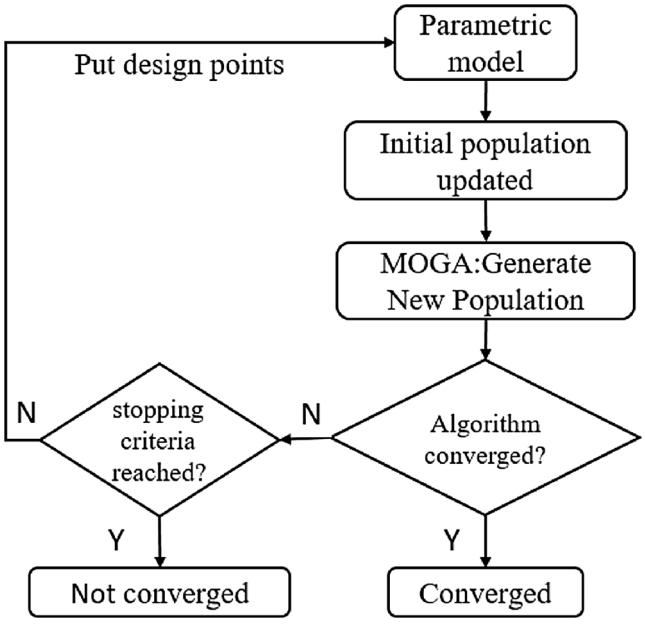

Fig. 5. Flow chart of the best solution for optimizing the blade– fixture.

To solve the above problems, the scalar optimization method is generally adopted, so that all the objective functions have their own minimum values. That is, the minimum value is scaled, as follows:

$$\min f_{(x)} = f_i^* x \in X\, i = 1,\ \ldots, k \quad (3.15)$$

where f_i^* is the scaled minimum value of an individual i. Therefore, the most ideal multi-objective optimization problem can be regarded as the vector f^*, expressed as follows:

$$f^* = (f_i^*, \ldots, f_k^*)^i \quad (3.16)$$

where f is determined to be the most advantageous.

Although the scalar sequence can solve many problems, the ideal vector is often not established, and the Pareto optimal solution is proposed. That is, in the vector space, there is a point $x' \in X$ that is superior to any solution, and it is called Pareto's best. Generally, there are multiple Pareto optimal solutions in the optimization. The number of Pareto's best advantages and the advantage level can be selected to solve this multi-objective optimization problem.

4. Experimental exploration

As shown in Fig. 2, the computer-aided technical system for fixture design and evaluation mainly included the positioning error transfer model, the FEM of the blade–fixture system and the optimization model of the blade–fixture layout. It is necessary to experimentally verify that the above models are feasible. The fixture verification experiments included geometric positioning error experimental analysis, mechanical behavior experiment of the blade–fixture system, and fixture layout design optimization test experiments. Finally, the fixture of another blade (test blade) was designed based on the computer aided fixture design and evaluation method, and the corresponding cutting experiments were carried out to verify the feasibility of this computer-aided fixture design and evaluation method by measuring the displacement response of the CNC machining process and the surface quality of the blade after cutting.

4.1. Geometric positioning experiment

The laboratory equipment mainly comprised the following: two test blades, and four dial indicators that were used to measure the displacement caused by the positioning point. Four size-changing positioning blocks, where the z-direction float of each positioning block was 1 mm, were used to examine the influence of the positioning block's height fluctuation in the z-direction on the positioning accuracy.

The test part was a third-stage blade of a jet engine with a bounding size of 220 × 100 × 5 mm. The tenon root of blade will require a high machining accuracy after removing much material. Therefore, the focus of this experiment is tenon root CNC machining. An investigation of the proposed fixture was implemented to examine the positioning performance.

To verify the positioning error caused by the manufacturing error of the four positioning elements on the blade profile surface, experiments were performed according to the following method. First, the blade was installed in the fixture according to the process specification, ensuring that the positioning block and the blade were in full contact.

Second, the positioning block A was replaced by a new positioning block which the z-direction height was increased by 1 mm. Third, the displacements of the four points (S_1, S_2, S_3, and S_4) of the blade were measured. Finally, the effects of the four positioning blocks (A, B, C and D) on the errors of the four positioning points (S_1, S_2, S_3, and S_4) of the blade were calculated, and the results were compared with the numerical modeling method of the positioning error. The experimental setup is shown in Fig. 6.

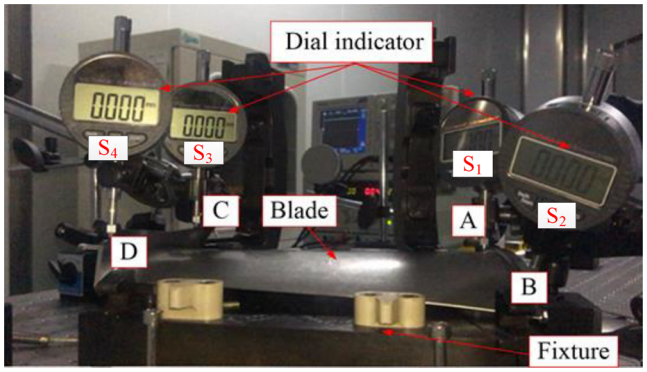

Fig. 6. Experimental setup for positioning error tests.

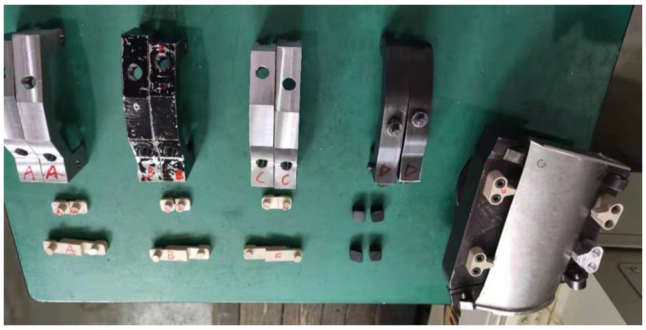

Fig. 7. Four different sets of fixture layouts.

4.2. Mechanical behavior experiment of blade–fixture system

To verify that the optimized fixture exhibited good mechanical behavior, cutting experiment analysis of the fixture was performed. Fig. 7 shows the fixture structure of different positioning positions. Four sets of typical positions were used for the cutting comparison experiment. Fixture C was designed according to the optimized positioning point.

The experimental site is shown in Fig. 8. The laser displacement sensor, which had a high sampling frequency and resolution, was used to measure the displacement response signal of the fixture during the cutting process. The acceleration displacement sensor was used to measure the vibration displacement signal of the blade–fixture system during the cutting process. The cutting experiment equipment mainly included an emulsion-cooling vertical machining center (KIV Hi-CENTER H40), a hard-alloy flat-end four tooth cutter, with a 16-mm diameter, and a Kistler rotary dynamometer [9]. A set of fixtures of the blade were used for comparison experiments to explain the mechanical behavior of the fixture and to verify the proposed computer-aided design algorithm and model.

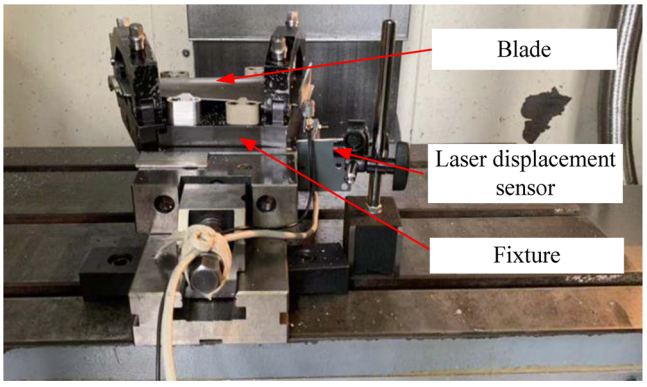

Fig. 8. Experimental setup.

During the cutting process, four sets of typical fixture will CNC machined by the same cutting process parameters to obtain the same cutting force, and the displacement response of different fixture will be comparatively analyzed to reflect the change of fixture stiffness.

4.3. Blade CNC machining processing experiment

To experimentally verify that the above models were feasible, a first-stage rotor blade of a low-pressure compressor in a jet engine, with a bounding size of 110 × 50 × 5 mm, was used to verify the computer-aided fixture design and evaluation method. The optimal fixture layout of the blade was first obtained by the proposed fixture layout optimization algorithm. The static performance of the fixture was analyzed, and the laboratory equipment mainly comprised the following: a blade, a fixture that was designed and manufactured using the proposed fixture layout optimization algorithm, and three dial indicators, which were used to measure the displacement caused by the clamping and unloading processes.

Fig. 9 shows the experimental site of the fixture calibration test. First, the blade was clamped in the correct position based on the clamping sequence. Second, the blade was unloaded, and the clamping force was reduced until the blade was completely loosened. The displacements of the six observation points on the blade (see Fig. 9(b)) were tested by dial indicators. This experiment was repeated three times to determine the consistency of the blade clamping process, and the displacement changes of the six points on the blade were compared to determine whether the blade had locally deformed. The performance of the fixture was finally analyzed based on the experimental data.

Fig. 10 shows the cutting performance test of the fixture. The purpose of the experiment was to apply the fixture to the production of a blade. The cutting experiment was carried out on a five-axis machining center using a six-tooth flat-bottomed cutter.

A laser displacement sensor and vibration acceleration sensor were used to detect the displacement and vibration responses during the cutting process, respectively, and to select a reasonable combination of process parameters using the magnitude of the response displacement and the amplitude of the vibration as a reference value.

The surface roughness of the blade was finally measured by a Marsurf XT20 surface roughness tester (Fig. 10(b)), which could not only measure the two-dimensional roughness parameter value of the machined surface but also scan the three-dimensional (3D) shape of the surface. In the surface roughness measurement process, the surface roughness value which is perpendicular to the cutter feed direction was measured. The surface roughness value was the average value of five measurements to ensure measurement accuracy.

5. Results and discussion

5.1. Analysis of fixture positioning error

The reliability of the numerical modeling and solution method of the positioning error was verified by comparative of calculated and experimental verification.

The analysis 3D model is shown in Fig. 11. The input conditions for this analysis are the change value of the positioning blocks (A, B, C, and D), and the outputs are the position deviations at the four positions (S_1, S_2, S_3, and S_4) (see Fig. 11 (b)). In order to verify the feasibility of the analysis method, the height of the positioning block increases by 1 mm to calculate the position change of the four positions (S_1, S_2, S_3, and S_4), and the corresponding tests are performed.

Table 2 is the calculation results of positioning error. Firstly, the original position values of S_1, S_2, S_3, and S_4 respectively are recorded, and these values can be obtained by measuring the size of the 3D model before the change of the positioning block. Secondly, the height of the positioning block A is increased by 1 mm, and the positioning change value of S_1, S_2, S_3, and S_4 are calculated through geometric constraints.

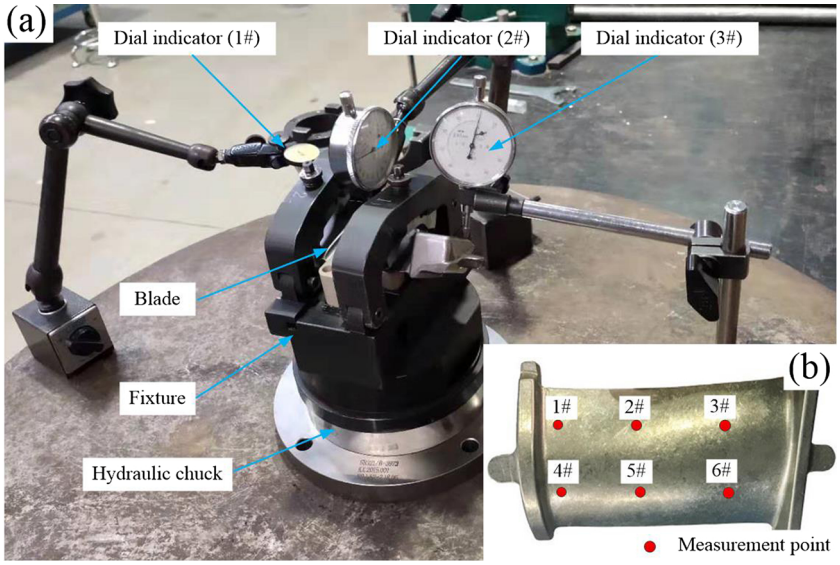

Fig. 9. Static test of fixture for the first rotor blade: (a) test setup and (b) measurement points.

Specifically, in Table 2, the original value of S_1 is 146.16 mm, and this value is 144.59 mm when the positioning block (A) increases by 1 mm, and the change amount of this value is 1.57 mm. Therefore, the position of the blade (S_1) is increased by 1.57 mm, and the position of the blade (S_2) is increased by -0.13 mm, and the position of the blade (S_3) is increased by 0.47 mm, and the position of the blade (S_4) is increased by -0.42 mm when the positioning block A is increased by 1 mm. The other positions of the blade (S_1, S_2, S_3, and S_4) are obtained by the same method when the positioning blocks (B, C and D) are increased by 1 mm, and the analysis results are shown in Table 2.

Table 3 shows the test results of position change of S_1, S_2, S_3, and S_4 when the height of the positioning block A is increased by 1 mm, and the height of the other positioning blocks (B, C and D) will be the original value. these values can be obtained through four dial indicators.

Specifically, in Table 3, the position change value of S_1 in the first blade is 1.482 mm, and the position change value of S_2 is -0.124 mm, and the position change value of S_3 is 0.477 mm, and the position change value of S_4 is -0.294 mm when the positioning block (A) increases by 1 mm, in fact, in the experiment, the increase amount of the positioning block A is close to 1 mm. In the second experiment on the second blade, the four values obtained are respectively 1.524 mm, -0.13 mm, 0.47 mm and -042 mm, which shows that the two experiments are highly consistent. The results of the repeated experiment blade are measured by the same method, and the analysis results are shown in Table 3.

Table 4 shows the test results of position change of S_1, S_2, S_3, and S_4 when the height of the positioning block B is increased by 1 mm, and the height of the other positioning blocks (A, C and D) will be the original value. These values can be obtained through four dial indicators.

Specifically, in Table 4, the position change value of S_1 in the first blade is -0.205 mm, and the position change value of S_2 is 1.527 mm, and the position change value of S_3 is -0.585 mm, and the position change value of S_4 is 0.378 mm when the positioning block (A) increases by 1 mm. The results of the repeated experiment blade are measured by the same method, and the analysis results are shown in Table 4.

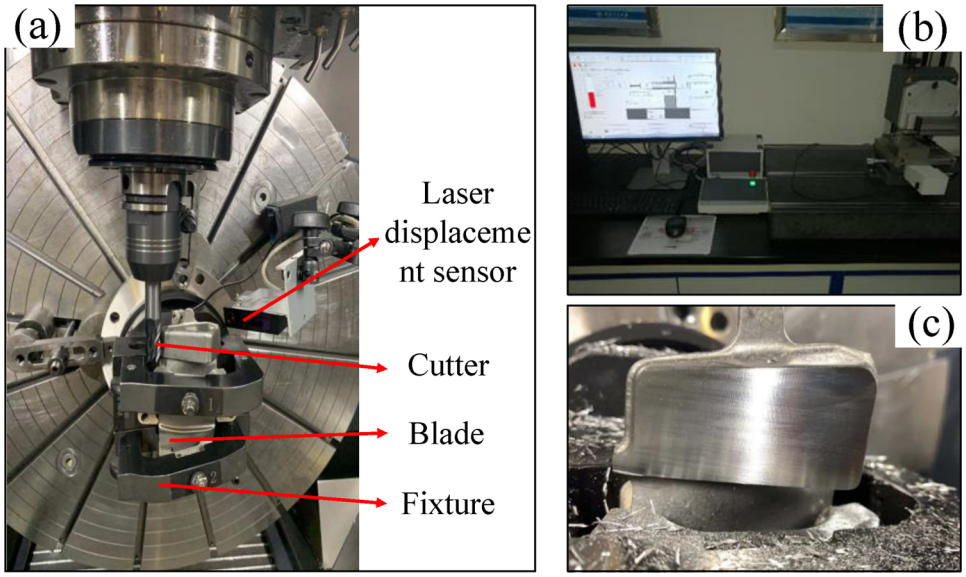

Fig. 10. Mechanical performance analysis of the fixture for the first rotor blade: (a) five-axis machining center, (b) Marsurf XT20 surface roughness tester fixture, (c) The machined blade tenon root surface.

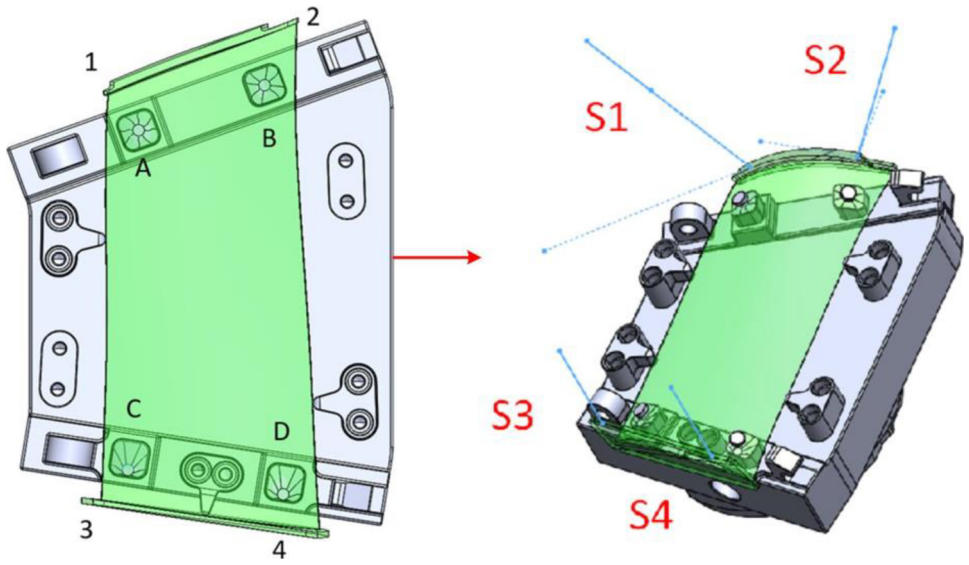

Fig. 11. Positioning block and positioning error response test direction: (a) positioning blocks (A—D) in fixture, (b) positioning error response test direction (S_1—S_4).

Table 2
Calculation results of positioning error.

Calculated	S_1 / mm	S_2 / mm	S_3 / mm	S_4 / mm
Original value	146.16	128.29	72.01	70.48
Positioning block A increases by 1 mm	144.59	128.42	71.54	70.9
Variable	1.57	−0.13	0.47	−0.42
Positioning block B increases by 1 mm	146.39	127	72.49	70.17
Variable	−0.23	1.29	−0.48	0.31
Positioning block C increases by 1 mm	146.51	128	71.01	70.06
Variable	−0.35	0.29	1	0.42
Positioning block D increases by 1 mm	146.06	128.6	71.76	69.48
Variable	0.1	−0.31	0.25	1

Table 3
Positioning error test results when changing the height of positioning block A.

Measuring position	S_1 / mm	S_2 / mm	S_3 / mm	S_4 / mm
Blade 1#	1.482	−0.124	0.477	−0.294
Blade 2#	1.524	−0.096	0.484	−0.358
Calculation results	1.57	−0.13	0.47	−0.42

Table 4
Positioning error test results when changing the height of positioning block B.

Measuring position	S_1 / mm	S_2 / mm	S_3 / mm	S_4 / mm
Blade 1#	−0.205	1.527	−0.585	0.378
Blade 2#	−0.183	1.447	−0.557	0.361
Calculation results	−0.23	1.29	−0.48	0.31

Table 5
Positioning error test results when changing the height of positioning block C.

Measuring position	S_1 / mm	S_2 / mm	S_3 / mm	S_4 / mm
Blade 1#	−0.28	0.289	0.924	0.338
Blade 2#	−0.277	0.275	0.888	0.329
Calculation results	−0.23	1.29	−0.48	0.31

Table 5 shows the test results of position change of S_1, S_2, S_3, and S_4 when the height of the positioning block C is increased by 1 mm, and the height of the other positioning blocks (A, B and D) will be the original value. these values can be obtained through four dial indicators.

Specifically, in Table 5, the position change value of S_1 in the first blade is -0.28 mm, and the position change value of S_2 is 0.289 mm, and the position change value of S_3 is 0.924 mm, and the position change value of S_4 is 0.338 mm when the positioning block (C) increases by 1 mm. The results of the repeated experiment blade are measured by the same method, and the analysis results are shown in Table 5.

Table 6 shows the test results of position change of S_1, S_2, S_3, and S_4 when the height of the positioning block D is increased by 1 mm, and the height of the other positioning blocks (A, B and C) will be the original value, and these values can be obtained through four dial indicators.

Specifically, in Table 6, the position change value of S_1 in the first blade is 0.074 mm, and the position change value of S_2 is -0.362 mm, and the position change value of S_3 is 0.291 mm, and the position change value of S_4 is 1.107 mm when the positioning block (D) increases by 1 mm. The results of the repeated experiment blade are measured by the same method, and the analysis results are shown in Table 6.

As shown in Fig. 12, the positioning errors obtained by the calculated and experimental methods were compared. Fig. 12(a)–(d) shows the displacement of four points (S_1, S_2, S_3, and S_4) on the blades mainly caused by the variation of positioning block A—D in the *z*-direction. The calculated results were basically the same as the two sets of experimental results. Thus, it was concluded that the above modeling method was reliable and could be used to describe the positioning errors caused by positioning element errors. Therefore, we can obtain an empirical model for the total positioning error on the positioning element errors by this numerical calculated modeling method

To analyze the coupling effect of positioning element errors on the total positioning error, an orthogonal design with four factors and three

Table 6
Positioning error test results when changing the height of positioning block D.

Measuring position	S_1 / mm	S_2 / mm	S_3 / mm	S_4 / mm
Blade 1#	0.074	−0.362	0.291	1.107
Blade 2#	0.074	−0.384	0.291	1.127
Calculation results	0.1	−0.31	0.25	1

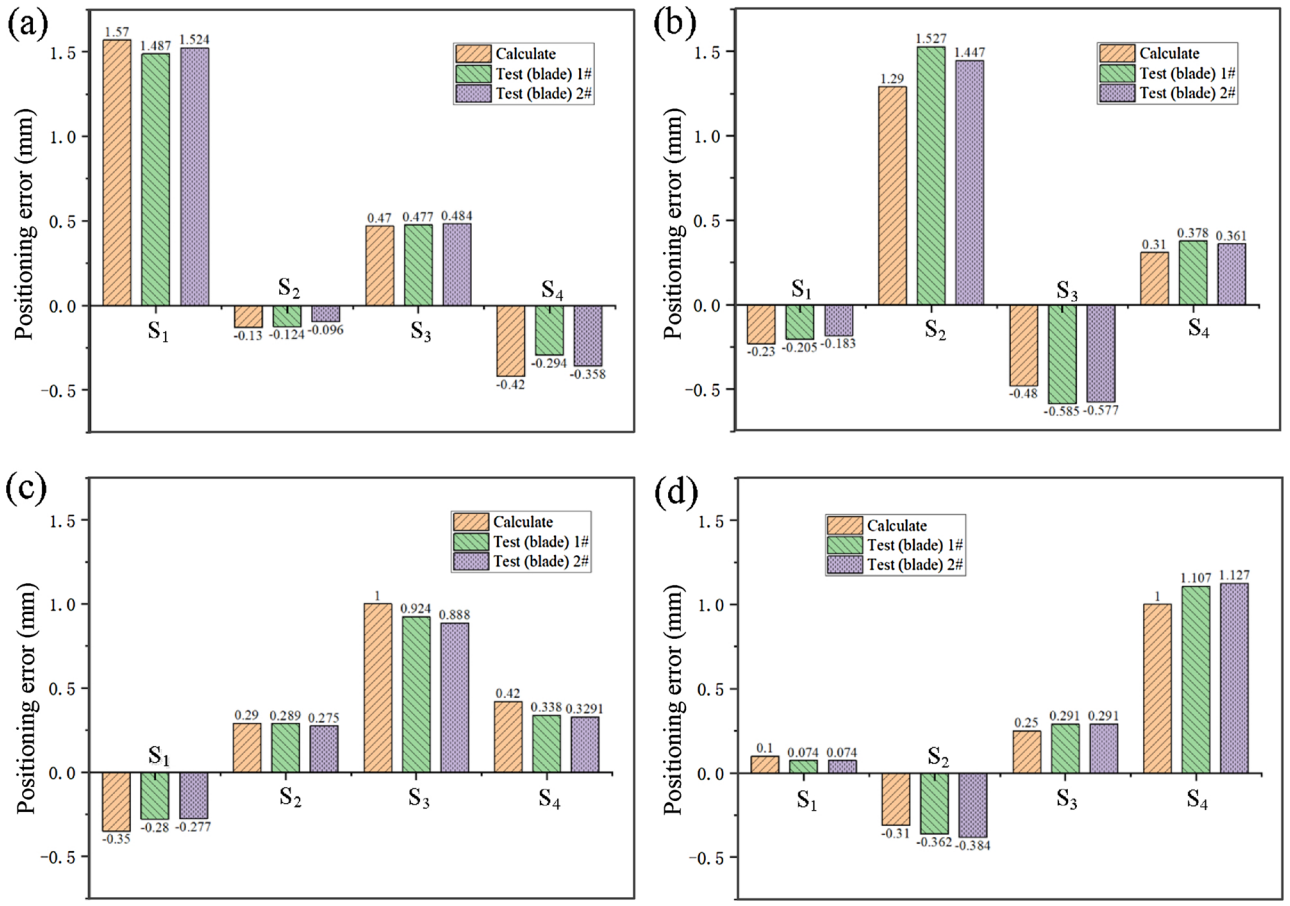

Fig. 12. Comparison of the numerical method and experiment: positioning error response of (a) S_1 (b) S_2, (c) S_3, and (d) S_4 with the change of the positioning block (A—D).

Table 7
Level of factors distribution of positioning element errors.

Level	Positioning block A / mm	Positioning block B / mm	Positioning block C/ mm	Positioning block D/ mm
−1	0	0	0	0
0	0.1	0.1	0.1	0.1
1	0.2	0.2	0.2	0.2

levels (L_4^3) was developed for the simulation analysis [22]. There were four main positioning element errors that affected total positioning error: positioning blocks A, B, C, and D. The total positioning error was described by the displacement of four points (S_1, S_2, S_3, and S_4) on the blade, as shown in Fig. 6. The test factor level table is shown in Table 7.

The purpose of the model analysis of the positioning element errors was to understand the interactions between the assessment indicators and influencing factors and to analyze the positioning errors. First, an orthogonal experiment was designed. Second, the positioning errors were calculated by numerical modeling. Finally, the empirical model of the total positioning errors based on the positioning element errors was established.

The final design of the orthogonal experiments with three factors and three levels and the calculation results are summarized in Table 8.

A statistical principle was used to establish the functional relationship between total positioning error and positioning element errors based on the experiments and experience. In actual production, based on a large number of tests and data analysis, there is a linear relationship between total positioning error and positioning element errors, as follows:

$$z_i = a_i + \sum_j b_{ij}x_j + \sum_j c_{ij}x_j^2 + \sum_{j,k} d_{j,k}x_j x_k \tag{5.1}$$

where z_j (j = 1,2,3 and 4) is the positioning error, that is, the displacement changes of the four points on the blade (S_1, S_2, S_3, and S_4), which is referred to as "closed-loop" in the positioning error analysis, as shown in Fig. 6. x_i (i = A, B, C, and D) is the variation of the positioning block (A, B, C, and D) in the z- direction, which is referred to as "component-loop" in positioning error analysis. a_i, $b_{i,j}$, $c_{i,j}$, and $d_{j,k}$ are undetermined coefficients.

The empirical model of the total positioning error on the positioning element errors was established based on the linear regression analysis and the final empirical model was established as follows:

$$\left.\begin{aligned} z_1 &= 0.000093 + 0.543x_1 + 0.489x_2 + 0.608x_3 - 0.637x_4 \\ z_2 &= -0.000016 + 0.651x_1 + 0.589x_2 - 0.504x_3 + 0.264x_4 \\ z_3 &= -0.000032 - 0.0211x_1 - 0.0384x_2 + 1.23x_3 - 0.115x_4 \\ z_4 &= -0.000093 - 0.0528x_1 - 0.0488x_2 - 0.118x_3 + 1.22x \end{aligned}\right\} \tag{5.2}$$

The confidence coefficient was set as a = 0.05. The significance of the model was tested by an F-test and a multiple correlation coefficient test method. $F = 3\left.\begin{aligned} z_1 &= 0.000093 + 0.543x_1 + 0.489x_2 + 0.608x_3 - 0.637x_4 \\ z_2 &= -0.000016 + 0.651x_1 + 0.589x_2 - 0.504x_3 + 0.264x_4 \\ z_3 &= -0.000032 - 0.0211x_1 - 0.0384x_2 + 1.23x_3 - 0.115x_4 \\ z_4 &= -0.000093 - 0.0528x_1 - 0.0488x_2 - 0.118x_3 + 1.22x \end{aligned}\right\} 3.63263 > F_{0.01}$ (4, 9-4-1) = 15.98. The multiple correlation coefficient was R = 0.9819193, and its minimum value was $Rmin$ = 0.930. Therefore, $R > Rmin$. The F-test and multiple correlation coefficient test confirmed that the established empirical model of positioning error fit well with the test data.

Sensitivity is the ratio of the variation of the total positioning error to the positioning element errors [22]. The value of the sensitivity

Table 8
Orthogonal experiment table and calculation results.

Number	A/ mm	B/ mm	C/ mm	D/ mm	S_1 / mm	S_2 / mm	S_3 / mm	S_4 / mm
1	0	0	0	0	0	0	0	0
2	0	0	0.1	0	0.061	−0.05	0.13	−0.012
3	0.1	0	0	0	0.054	0.065	−0.006	−0.005
4	0	0	0	0.1	−0.064	0.026	−0.019	0.122
5	0	0.1	0	0	0.049	0.059	−0.005	−0.005
7	0	0	0.2	0	0.122	−0.101	0.261	−0.024
8	0.2	0	0	0	0.109	0.13	−0.012	−0.011
9	0	0	0	0.2	−0.127	0.053	−0.039	0.243
10	0	0.2	0	0	0.098	0.118	−0.01	−0.01
11	0	0.1	0.1	0	0.11	0.008	0.125	−0.017
12	0.1	0	0	0.1	−0.009	0.092	−0.025	0.116
13	0.1	0.1	0	0	0.103	0.124	−0.011	−0.01
14	0	0.1	0	0.1	−0.015	0.085	−0.025	0.117
15	0.1	0	0.1	0.1	0.051	0.041	0.105	0.105
16	0.1	0.1	0.1	0	0.164	0.074	0.119	−0.022
17	0	0.1	0.1	0.1	0.046	0.035	0.106	0.105
18	0.1	0.1	0	0.1	0.04	0.15	−0.03	0.111
19	0.1	0.1	0.1	0.1	0.1	0.1	0.1	0.1

determine whether the positioning element errors are significant or insignificant. In this study, z_j (j = 1, 2, 3, and 4) was closed-loop, and x_i (i = A, B, C, and D) was component-loop. Thus, the sensitivity analysis method could determine the degree of influence of each component loop on the closed-loop and determine whether the component-loop (A, B, C, and D) was significant.

If the objective function is $f(x)$ and its variables are $x = (x_1, x_2, x, \ldots, x_n)$, and if $f(x)$ is differentiable, the sensitivity can be calculated as follows [22]:

$$S(x_i) = \frac{\partial f(x)}{\partial x_i} \tag{5.3}$$

Based on Eq. (5.3), the sensitivity of the total positioning error to positioning block A is as follows:

$$\left.\begin{aligned} S_1(x_1) &= \frac{\partial z_1}{\partial x_1} = 0.543 \\ S_2(x_1) &= \frac{\partial z_2}{\partial x_1} = 0.651 \\ S_3(x_1) &= \frac{\partial z_3}{\partial x_1} = -0.0211 \\ S_4(x_1) &= \frac{\partial z_4}{\partial x_1} = -0.0528 \end{aligned}\right\} \tag{5.4}$$

The sensitivity of the total positioning error to positioning block B is as follows:

$$\left.\begin{aligned} S_1(x_2) &= \frac{\partial z_1}{\partial x_2} = 0.489 \\ S_2(x_2) &= \frac{\partial z_2}{\partial x_2} = 0.589 \\ S_3(x_2) &= \frac{\partial z_3}{\partial x_2} = -0.0384 \\ S_4(x_2) &= \frac{\partial z_4}{\partial x_2} = -0.0488 \end{aligned}\right\} \tag{5.5}$$

The sensitivity of the total positioning error to positioning block C is as follows:

$$\left.\begin{aligned} S_1(x_3) &= \frac{\partial z_1}{\partial x_3} = 0.608 \\ S_2(x_3) &= \frac{\partial z_2}{\partial x_3} = -0.504 \\ S_3(x_3) &= \frac{\partial z_3}{\partial x_3} = 1.23 \\ S_4(x_3) &= \frac{\partial z_4}{\partial x_3} = -0.118 \end{aligned}\right\} \tag{5.6}$$

The sensitivity of total positioning error to positioning block D is as follows:

$$\left.\begin{aligned} S_1(x_4) &= \frac{\partial z_1}{\partial x_4} = -0.637 \\ S_2(x_4) &= \frac{\partial z_2}{\partial x_4} = 0.264 \\ S_3(x_4) &= \frac{\partial z_3}{\partial x_4} = -0.115 \\ S_4(x_4) &= \frac{\partial z_4}{\partial x_4} = 1.22 \end{aligned}\right\} \tag{5.7}$$

The total sensitivity of closed-loop z_j (j = 1, 2, 3 and 4) to component-loop x_i (i = A, B, C, and D) is as follows:

$$\left.\begin{aligned} S_A &= \frac{\partial z_1}{\partial x_1} + \frac{\partial z_2}{\partial x_1} + \frac{\partial z_3}{\partial x_1} + \frac{\partial z_4}{\partial x_1} \\ S_B &= \frac{\partial z_1}{\partial x_2} + \frac{\partial z_2}{\partial x_2} + \frac{\partial z_3}{\partial x_2} + \frac{\partial z_4}{\partial x_2} \\ S_C &= \frac{\partial z_1}{\partial x_3} + \frac{\partial z_2}{\partial x_3} + \frac{\partial z_3}{\partial x_3} + \frac{\partial z_4}{\partial x_3} \\ S_D &= \frac{\partial z_1}{\partial x_4} + \frac{\partial z_2}{\partial x_4} + \frac{\partial z_3}{\partial x_4} + \frac{\partial z_4}{\partial x_4} \end{aligned}\right\} \tag{5.8}$$

Based on formulas (5.4–5.8), the total sensitivity of closed-loop z_j (j = 1, 2, 3 and 4) to component-loop x_i (i = A, B, C, and D) is as follows:

$$\left.\begin{aligned} S_A &= 1.2679 \\ S_B &= 1.1652 \\ S_C &= 2.46 \\ S_D &= 2.236 \end{aligned}\right\} \tag{5.9}$$

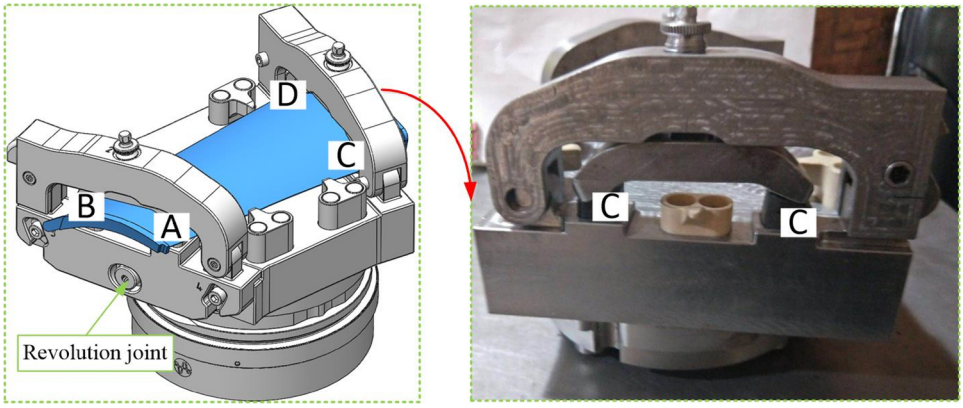

Fig. 13. Fixture structure: (a) fixture model, (b) experimental fixture.

Therefore, the total positioning error was mostly sensitive to positioning block C, followed by positioning blocks D, A, and B. In other words, component-loops C and D had the greatest impact on the total positioning error. This was because the support plate of positioning blocks A and B was a self-referenced structure, which made the total positioning error insensitive to the components on this plate, as shown in Fig. 13. Therefore, in the design of the fixture, the dimensional accuracy of positioning blocks C and D must be preferentially ensured. Furthermore, the tolerance requirements of these two positioning blocks (C and D) were higher than the others (A and B), and the tolerance variation range of these two positioning blocks (A and B) was smaller than others (C and D). In the fixture manufacturing process, the manufacturing accuracy of positioning blocks C and D must be preferentially ensured.

In this blade–fixture system, A, B, C, and D were the component-loops of the size chain. The position change in the z-axis direction of tenon root was the closed loop of this size chain, which was related to the dimensional accuracy of the positioning. Therefore, the closed loop was most sensitive to the component-loops C and D, which also indicated that the dimensions of component-loops C and D must be

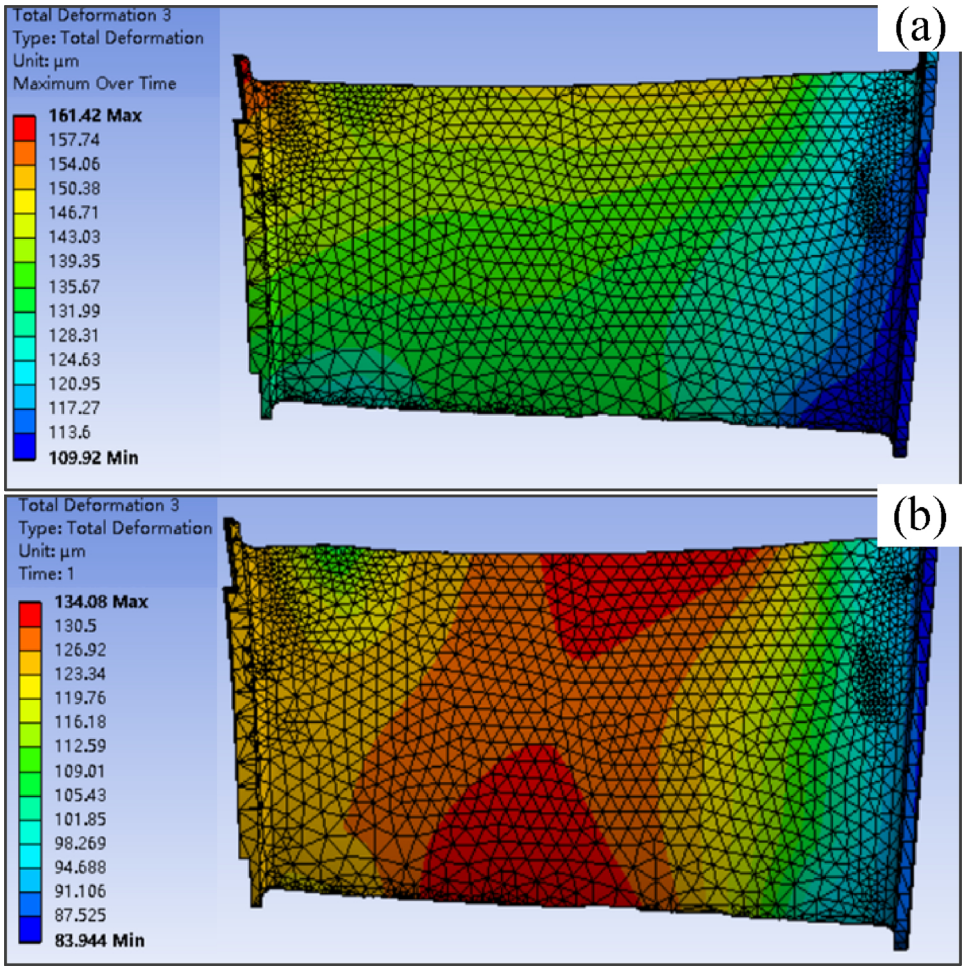

Fig. 14. Fixture structure: (a) deformation of the blade in the ideal clamping state and (b) deformation of the blade in the non-ideal clamping state (micron -scale manufacturing error).

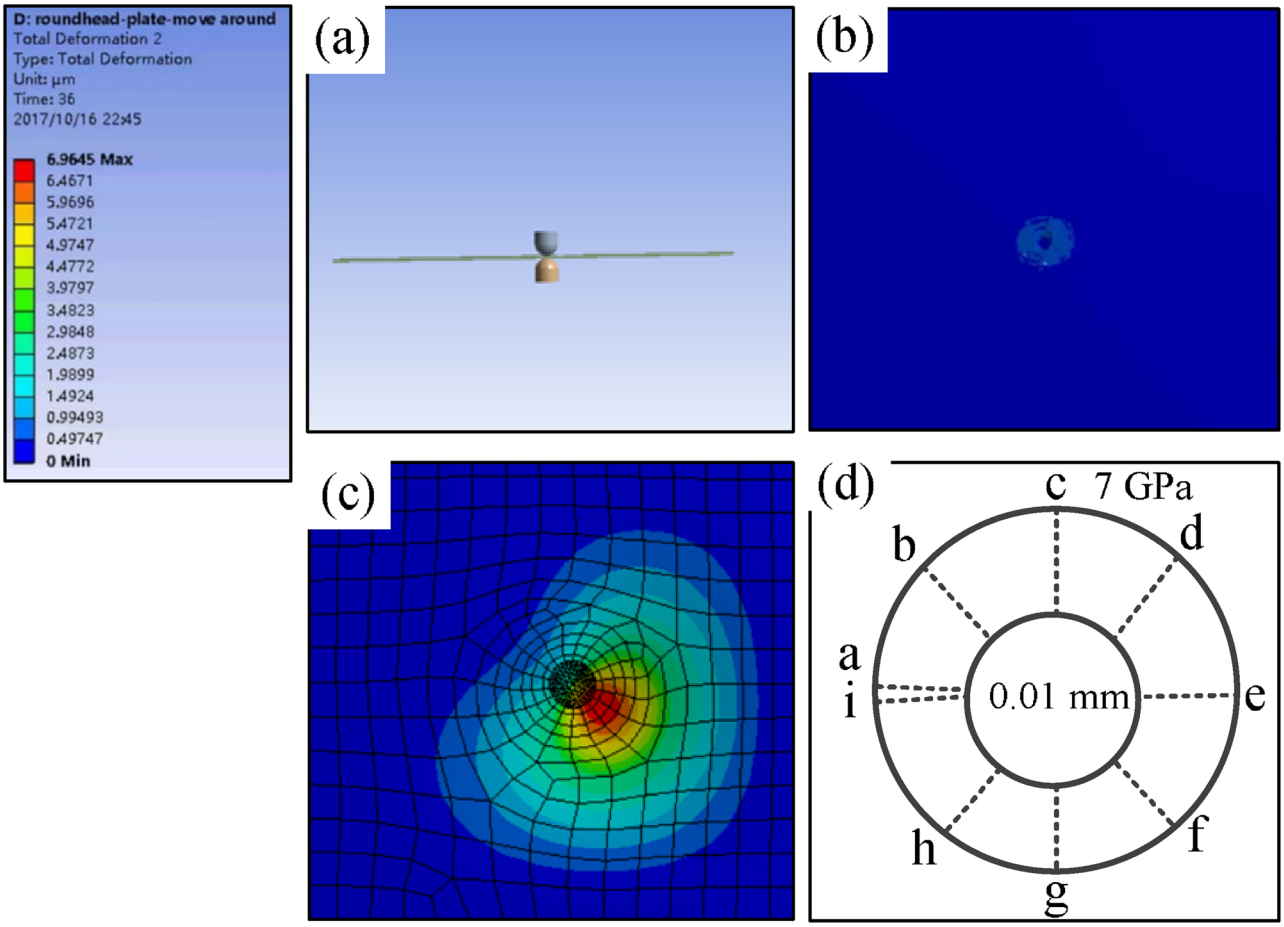

Fig. 15. Deformation variation: (a) 3D model, (b) deformation distribution of the ideal clamping state (no manufacturing error), (c) deformation distribution of the non-ideal clamping state (micron-scale manufacturing error), (d) distribution circle of deformation (convex and concave areas).

preferentially guaranteed. This method of computer-aided dimension analysis can provide guidance for the size control of the fixture design.

5.2. Mechanical behavior deformation analysis of fixture

Fig. 14 shows a deformation cloud diagram of the blade under the action of the clamping and cutting forces, and the clamping force was 2200 N in this case. The most important step in the FEM process is to determine the boundary conditions of the FEM, which have a great influence on the accuracy of the simulation. There have been many studies on the boundary conditions and modeling process of the FEM, and similar models and boundary conditions were used in this study [23].

Fig. 14(a) shows the deformation cloud diagram of the ideal clamping state of the blade. The blade deformation was an overall displacement change rather than a local deformation, which is consistent with previous literature analysis [23]. The overall deformation can be compensated by the corresponding adaptive algorithm, and the local deformation affected the final manufacturing accuracy of the blade, which had an adverse effect on the blade's fatigue life. For example, the local deformation could easily cause stress concentration and crack propagation. Therefore, local deformation is unfavorable and must be strictly avoided in the manufacture of blades.

However, in actual production process, the blade has a non-ideal deformation in this clamping scheme of this fixture (see Fig. 14(b)), and local deformation also appeared in the experiment. This was mainly caused by the manufacturing errors of the clamping element. Therefore, the deformation of the blade due to the manufacturing error of the clamping component must be considered. As with the positioning error analysis above, the error transformation of the positioning component had a significant influence on the positioning accuracy. Similarly, the small size error of the positioning and clamping elements had a significant impact on the mechanical properties of the blade–fixture system. In particular, Fig. 14(b) shows the deformation cloud diagram of non-ideal clamping conditions, where all clamping heads were offset from the center by 50 μm, and the positions of the positioning points did not change. The influence of the clamping position on the clamping deformation was very significant.

To analyze the deformation variations, a thin plate was used to analyze the deformation distribution, and this change trend reflected the influence of the actual manufacturing error of the fixture manufacturing. Assuming that there was no relative positional deviation between a pair of spherical clamping heads (Fig. 15(a)), the calculation indicated that a certain degree of deformation will occur in the vicinity of the pressed area, and the deformation tendency is shown in Fig. 15(b). Furthermore, considering that there may be a certain deviation between the positions of the pair of ball heads (Fig. 15(c)) and assuming that the deviation value was 0.01 mm, and the deformations obtained by the calculation are shown in Fig. 15(c).

A convex and concave area (see Fig. 16) appeared, and the distribution direction was the same as the connection line of the contact points of the two clamping heads due to the misalignment of the clamping heads. Thus, in the real case, if there is a certain degree of incomplete symmetry between the clamping and positioning heads due to the manufacturing error or design scheme, even if the amount of asymmetry is on the order of tens of micrometers, the unsatisfactory deviation will produce a high– low deformation zone in such thin-plate parts.

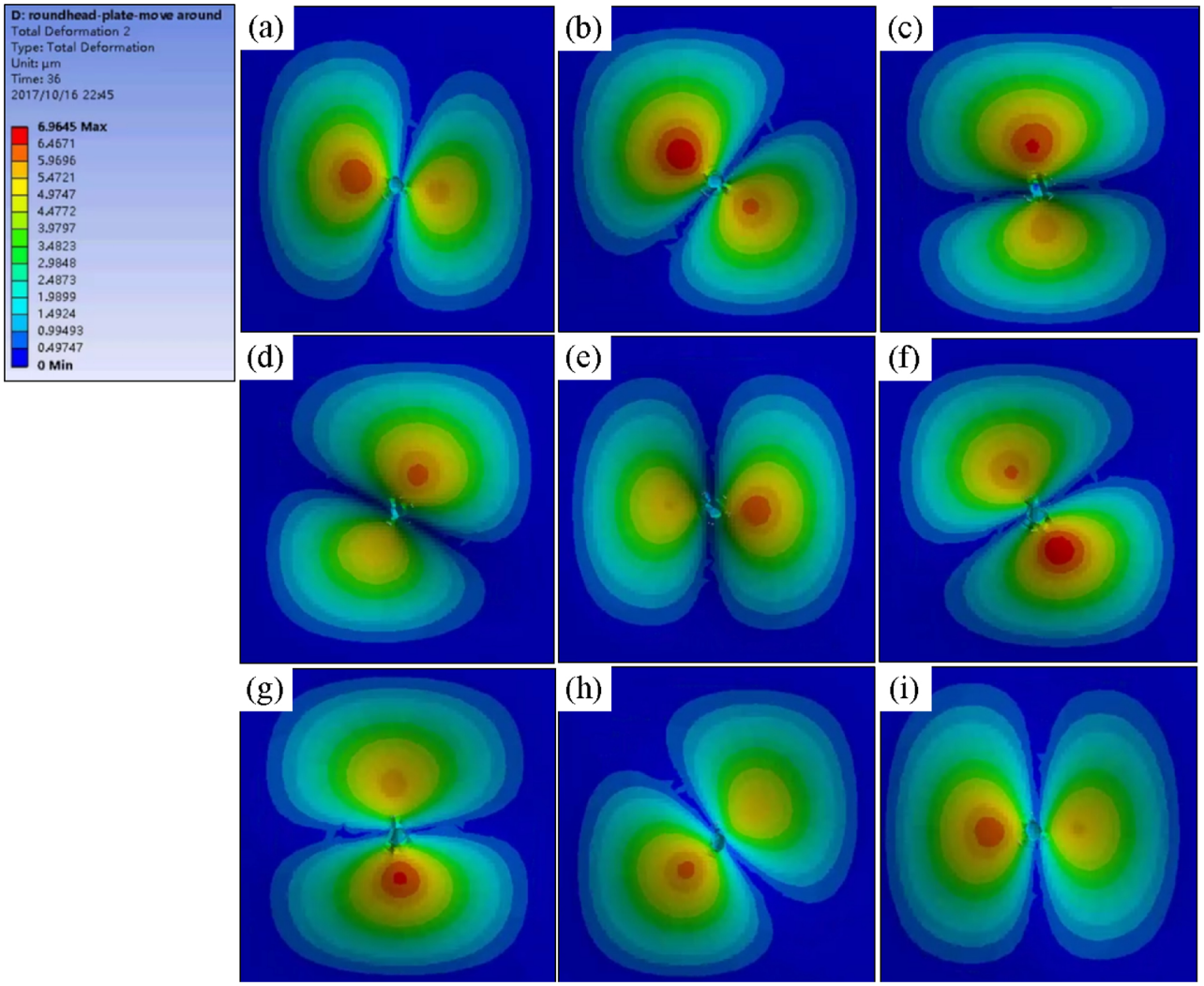

Fig. 16. Deformation variation corresponding to Fig. 15 (d) from a to g.

In the fixture design, especially considering the clamping method of the blade, the mechanical characteristics of the blade structure and the thin plate structure were similar. However, the clamping structure of blade used four pairs of positioning and clamping structures. Therefore, the four pairs of positioning and clamping heads used by the fixture scheme will be required for simulation analysis of the fixture structure. Supposing that there were certain positional deviations of the four clamping heads to the positioning heads, the deformation of thin-walled parts were simulated and analyzed by setting different offsets of the four points. A series of results were obtained, as shown in Fig. 17.

All possible offsets were simulated, the results were statistically analyzed (Fig. 17), and the distribution of deformation behaviors was obtained. First, the four clamping points were independent and did not directly affect each other. Each of them independently produced a concave– convex pair, and the four pairs of concave and convex points of the four points had a common influence on the deformation of the thin- walled part. Second, the degree of deformation was superimposed, and the deformation increased when two or more depressions/raised centers were distributed toward one position and vice versa. Finally, the edge of the thin-walled part was the most deformed part due to the absence of constraints. The analysis of these trends obtained by FEA were used to optimize the analysis of the four positioning points and clamping heads.

Researching in advanced manufacturing technology requires advanced detection systems, which will complement the results of the simulation analysis and theoretical analysis. In the CNC machining process of a blade tenon root, the cutting force will lead to deformation of the blade. Therefore, a displacement sensor test system with a high-resolution and high sampling frequency is necessary to monitor the influence of the high- frequency displacement signals caused by the high-frequency cutting force during CNC machining process, and the measured data will be able to guide the design of the fixture.

The blade deformation was the largest when the cutting force was applied at both ends of the blade tenon root [23]. Therefore, the deformation monitoring of the blade Tenon root during the CNC machining process is particularly important. The stiffness of blade–fixture system is sufficient if the maximum deformation of the blade Tenon root meets the machining accuracy requirements. However, it is known from experience that the blade will produce high-frequency vibration displacement signal under a high-frequency cutting force. Therefore, the dynamic response displacement signal test during the machining includes high-frequency vibration displacement signals and low-frequency deformation signals. The displacement sensor must exhibit high acquisition frequency, high resolution, high accuracy and low pollution. Eddy current displacement sensors and laser displacement sensors are suitable options.

Fig. 18(a) shows the spectrum signal of the cutting force after the FFT analysis, and Fig. 18(b) shows the displacement response signal after the FFT analysis during the cutting process obtained by the eddy current displacement sensor. The cutting force signal and the

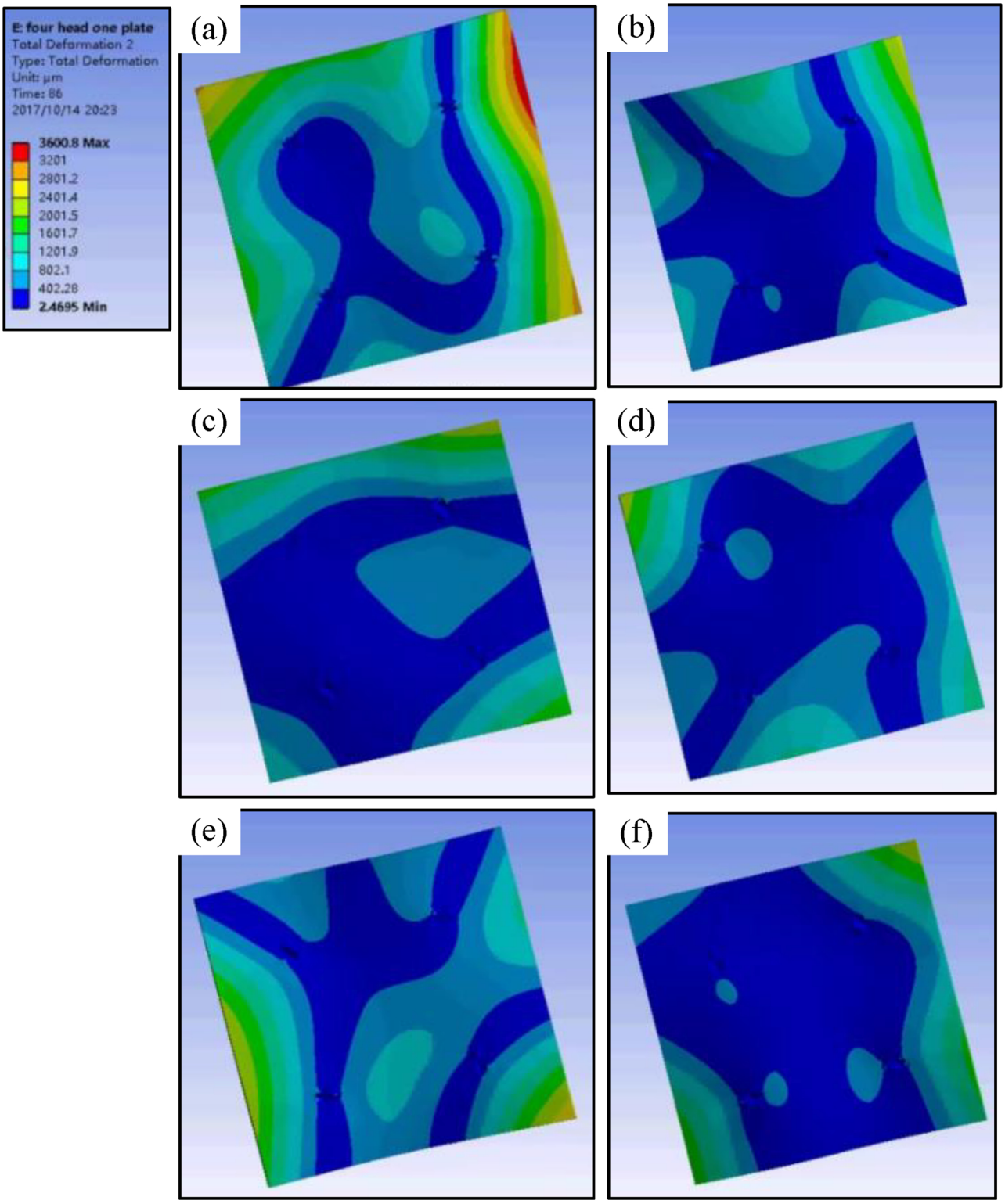

Fig. 17. Deformation trend of the thin- walled part.

displacement response signal have a spectral correspondence. Therefore, the displacement response signal obtained by the eddy current displacement sensor was decomposed into high- and low-frequency parts by FFT analysis, wherein the signal had a one-to-one correspondence between the cutting force frequency and the displacement response of the cutting force at the same frequency. The low frequency part was used as the elastic displacement of the blade before and after cutting, and the maximum value of the change reflected the system stiffness of the blade–fixture. This type of processing was consistent with the signal testing and analysis methods in the literature [23], and it can reflect the small displacement signals of the fixture system and the stiffness of the fixture system.

On the other hand, the laser displacement sensor has a higher measurement accuracy and resolution, and it can be used to measure the displacement signal. Thus, the vibration signal of the system can be measured by combining with an acceleration displacement sensor, and

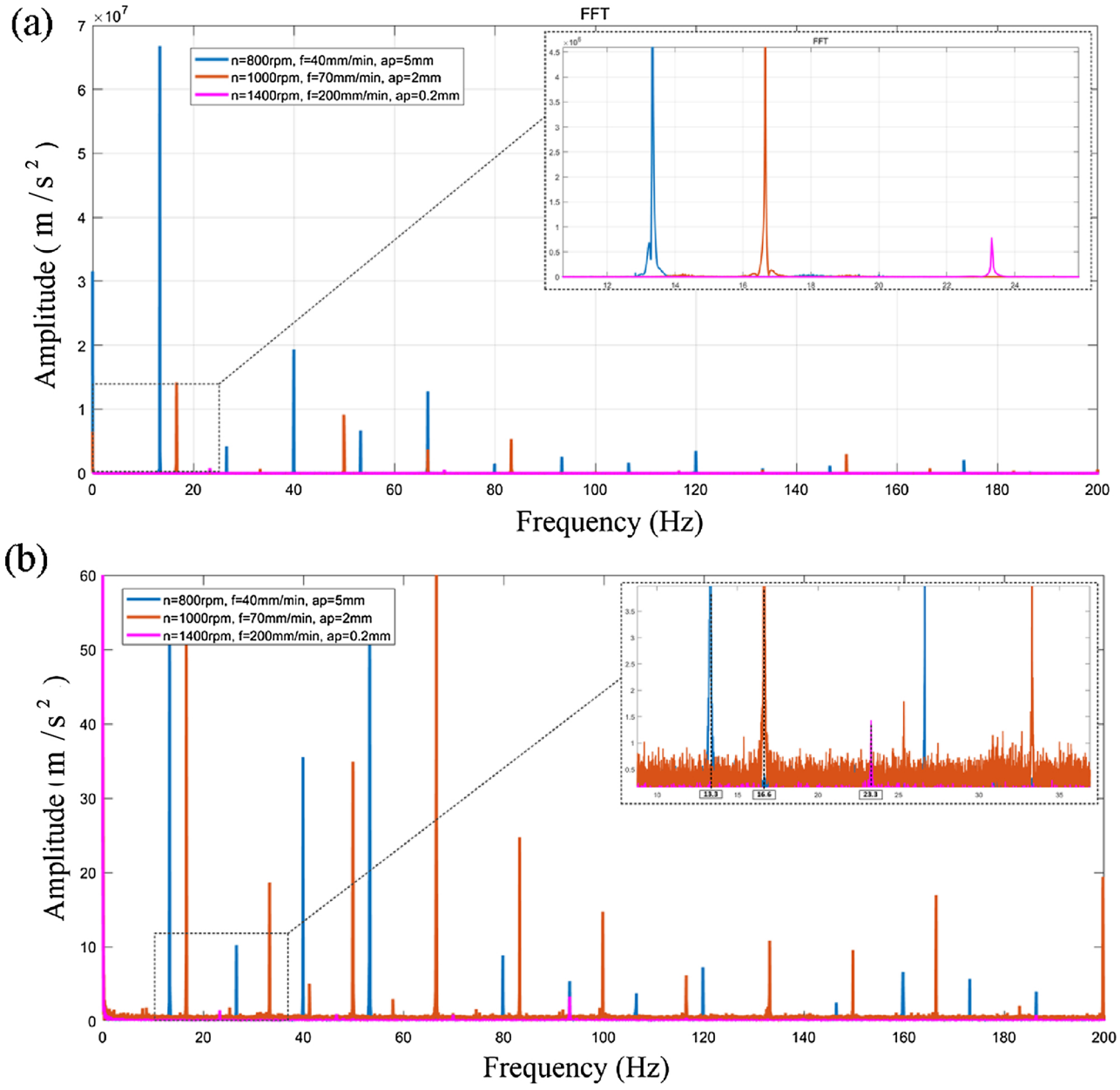

Fig. 18. Deformation trends: (a) cutting force FFT signal, (b) displacement response FFT signal obtained by eddy current sensor.

the system can be analyzed simultaneously based on the displacement variation, dynamic response, and magnitude of the vibration value.

Fig. 19(a) shows the displacement change signal obtained by the laser displacement sensor, and Fig. 19(b) shows the displacement change signal obtained by the vibration acceleration. The displacement signal obtained by the laser displacement sensor reflected the displacement of the system. In actual processing, the cutting force is a force that changes with time and position. This force can be obtained by a force sensor, and the maximum cutting force can be achieved throughout the total cutting time. The displacement response of the blade tenon corresponding to cutting force is also a displacement amount that changes with time and position. This displacement signal obtained by a laser displacement sensor is a monitored signal with the cutting force changing with time and position, and the maximum displacement during the entire time period can be obtained.

The acceleration sensor reflected the high-frequency vibrations of the blade–fixture system, and the blade vibration can be monitored to judge the stiffness of the fixture. It can be seen from the Fig. 19(b) that the vibration signal is relatively stable throughout the cutting process, and there is no obvious vibration phenomenon.

The combination of the laser and acceleration displacement sensors could better monitor the displacement and vibrations of the blade–fixture system. The laser displacement sensor can verify the optimal fixture layout obtained through static optimization, and the vibration displacement sensor can monitor the dynamic characteristics of the designed system.

Therefore, the experimental value used in this comparative analysis is obtained by a laser displacement sensor, and the high-frequency signal obtained by the vibration sensor will be used as a dynamic monitoring to determine whether the fixture involved meets the dynamic requirements.

Fig. 20 shows the mapping relationship of the cutting force and low-frequency displacement response obtained by the simulations and experiments. The maximum cutting force is used as the input of the FEA to obtain the deformation amount, which will be used as the simulation value of the deformation amount. The maximum deformation during

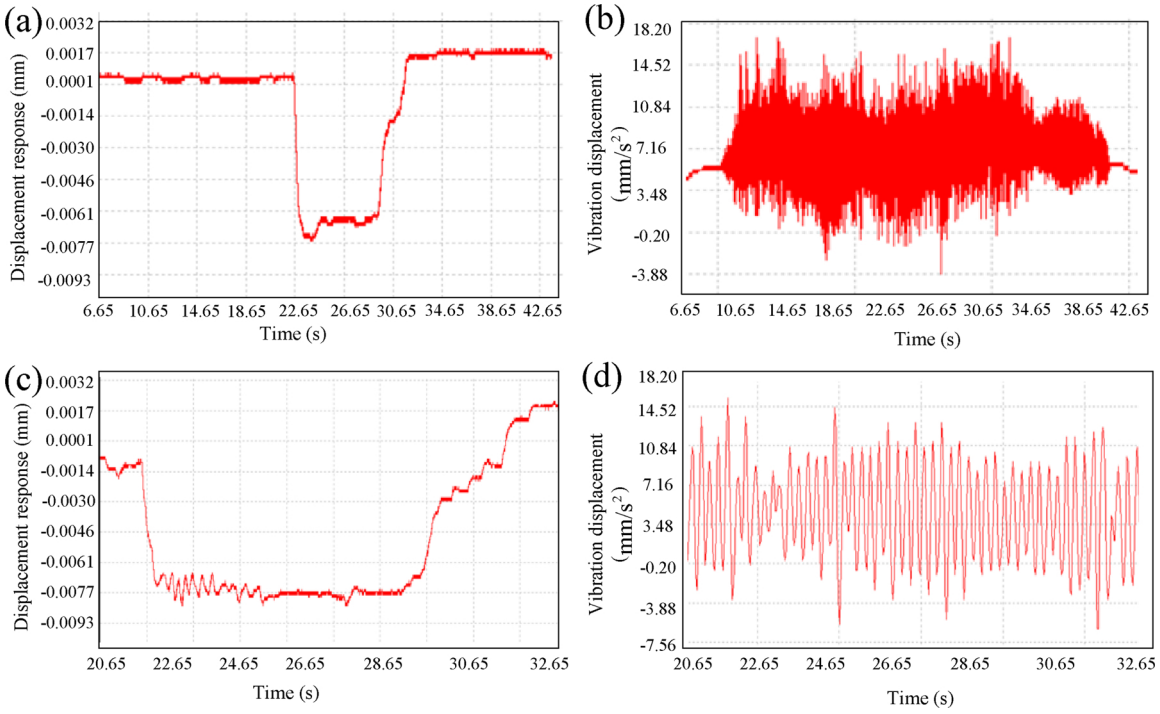

Fig. 19. Displacement response signal: (a) displacement response signal obtained by the laser displacement sensor, (b) displacement response signal obtained by the vibration acceleration sensor, (c) partial enlargement of Fig. 19 (a), (d) partial enlargement of Fig. 19 (b).

the entire cutting process can be obtained by a laser displacement sensor, and will be the experimental value of the deformation amount. The reliability of the simulation method is analyzed by comparing the simulation and experimental values.

As shown in Fig. 20, the overall trend of the actual experimental test value of the test system was the same as the simulated value. Both showed that the blade tenon root deformation increased with the increase in the cutting force. The similarity between the experimental and simulated values was higher than 50 %, There is indeed a certain deviation between the experimental values and the simulation. Therefore, the FEA method can give the changing trend to guide the design and analysis of the experiment. However, the experimental test results are still the main accurate value to design and development of fixture manufacturing.

There are mainly the following reasons causing deviations between experiment and simulation. Firstly, there is a contour error of the blade profile surface after precision forging process (near-net-shaped jet engine blades), and this error is the manufacturing error of the precision forging process (near-net-shaped jet engine blades), which is about 0.005 mm-0.08 mm. This error is ignored in the FEA, because this error is not a specific value on the blade body, and the specific value of the error at that specific point cannot be determined. This may be one of the main reasons for the difference between the simulated and experimental values (Fig. 20).

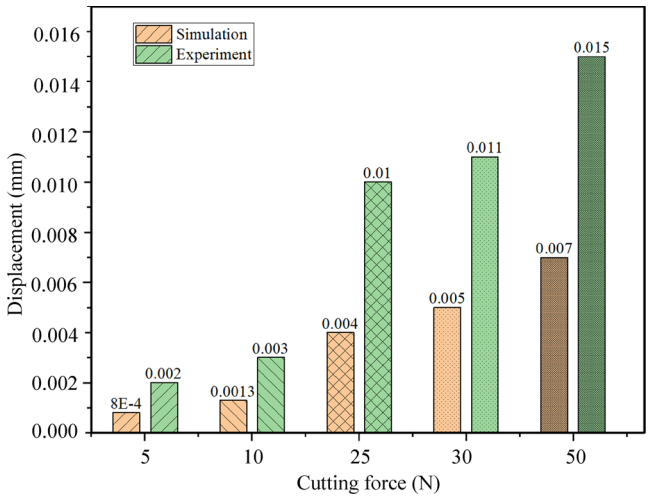

Fig. 20. Mapping relationship of the cutting force and low-frequency displacement response.

Secondly, the ideal contact conditions which ignores surface waviness, surface roughness are used in FEA [25]. However, in practice it is the non-ideal contact surface. This also leads to a difference between simulation and experimentation. However, the trend of experimentation and simulation is consistent.

Thirdly, in order to simplify the FEA process and obtain a large number of values, as the input sample points of the genetic algorithm, the static model instead of a dynamic model is used as the optimization model. There is a certain difference between the experiment and simulation, however the optimization fixture layout obtained in the static model layout, will have the excellent dynamic characteristics, which is reasonable in the changing trend.

Due to the above three conveniences, there is a large difference between the simulated and experimental values, however, the change trend between the simulated and experimental values is consistent.

Therefore, the construction of the high-resolution distortion test system could accurately monitor the displacement of the blade tenon root during the machining processing. This also indicated that the established FEA was reasonable, and the proposed computer-aided fixture design and evaluation method were feasible. This fixture mechanical analysis method was also reasonable and could be used to design and evaluate fixtures.

5.3. Analysis of fixture layout optimization

In this solution algorithm, there were 1298 data samples, and the convergence trend of the optimization algorithm (see Fig. 21) is well, and there was no local optimal solution.

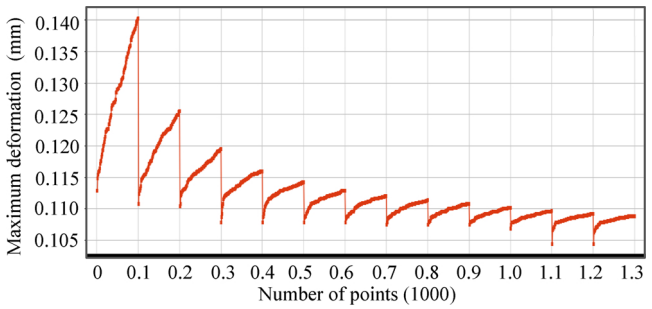

Fig. 21. Convergence trend of the genetic algorithm.

The optimized fixture layout obtained by the combination of the genetic algorithm and FEA, and three sets of Pareto advantage optimal solutions are shown in Table 9, and the blade deformation at these positioning points was the smallest. Candidate point #1 was the final blade–fixture layout point because it yielded the smallest blade deformation in these three Pareto advantage optimal solutions. Thus, the optimal fixture layout was obtained, which will produce the smallest blade deformation and the best blade–fixture system stiffness.

Fig. 22 shows the change in the displacement response signal during the cutting process. In this analysis, fixture C was obtained based on the optimization algorithm, and its positioning points were the Pareto advantage optimal solutions (candidate point #1 Table 9). Fixtures (A, B, and D) are comparison fixtures obtained through experience. Comparing the four fixtures, the displacement response of fixture C was the smallest. Therefore, the stiffness of fixture C was significantly higher than those of the other fixtures and was similar to the optimal solution obtained by the genetic algorithm and FEA. This also showed that the proposed fixture optimization design analysis method was reliable and the proposed computer-aided fixture layout optimization method could be used to guide the optimization design of the fixture.

5.4. Application verification of computer-aided fixture design and evaluation method

Fig. 23 shows a displacement response trend diagram of the first rotor blade in the unloaded state of the clamping force. In this experiment, the clamping force was gradually reduced from 2200 to 0 N, and the displacement responses at the six test points of the blade were obtained by dial indicators.

The displacements of these six measurement points were around 0.10 mm, which indicated that the displacements of these six points were simultaneously changed, no local loading occurred on the surface of the blade, and the loading force of the blade was evenly distributed and stable. The displacement response caused by the clamping force of the designed fixture was 0.10 mm, which indicated that the stiffness of the fixture was acceptable.

Fig. 24 shows the surface quality of the blade after CNC machining. The surface of the blade exhibited a texture due to the vibrations (Fig. 24(a)) when the blade process system possessed insufficient stiffness or the cutting process parameters were not properly selected. Such a blade surface is unacceptable and must be avoided. Fig. 24(b) shows the surface quality of the blade obtained in this experiment. The blade surface was smooth, and there was no evident vibration texture, which indicated that there were no significant vibrations during the blade CNC machining process, and the cutting process parameters and the process system were well matched. Therefore, the optimized process fixture and the experimental parameters were adequate which was acceptable for blades producing.

Fig. 25 shows the surface roughness test results of CNC machined blades. The surface roughness after the CNC machining process was below Ra 0.8 μm, and the surface roughness of some parts of the blade was below Ra 0.3 μm, which fully met the requirements of the cutting process for the final surface roughness. The obtained blade surface quality was acceptable, and the process equipment and process method could be used in actual industrial production.

Therefore, considering the displacement response caused by the unloading of the clamping force, the displacement response of the optimized fixture, and the surface roughness of the blade after CNC machining, the optimized fixture and CNC machining methods were feasible, and the fixture design and evaluation method proposed in this paper was reasonable, and this computer-aided fixture design and evaluation method can provide guidance in the production of blades.

Table 9
The optimized fixture layout.

Parameter	Candidate point #1	Candidate point #2	Candidate point #3
x_1	29.634	29.583	29.582
y_1	2.6693	2.7404	2.7402
x_2	31.174	31.092	30.829
y_2	1.4384	1.3685	1.5778
x_3	21.84	21.625	21.994
y_3	110.79	105.31	104.46
x_4	22.643	21.362	21.949
y_4	115.35	101	110.75
Deformation	0.10438	0.10618	0.10646

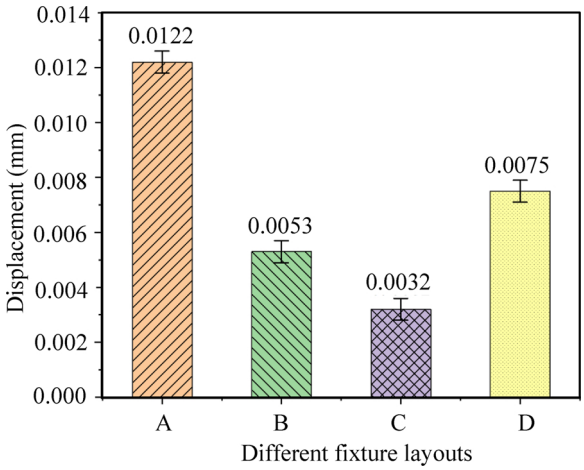

Fig. 22. Displacement response of different fixtures (A, B, C and D).

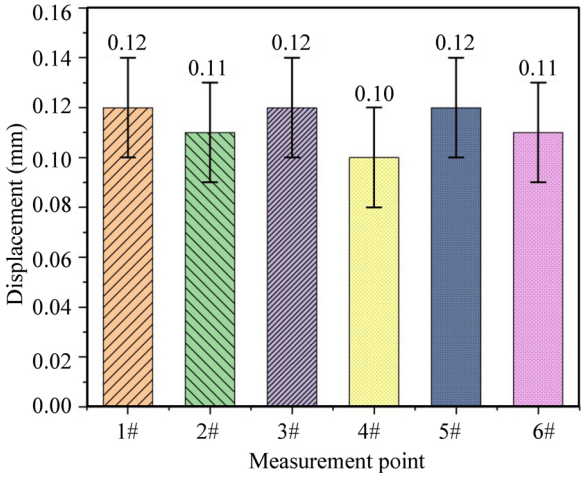

Fig. 23. Displacement of the first-stage rotor blade during the unloading process.

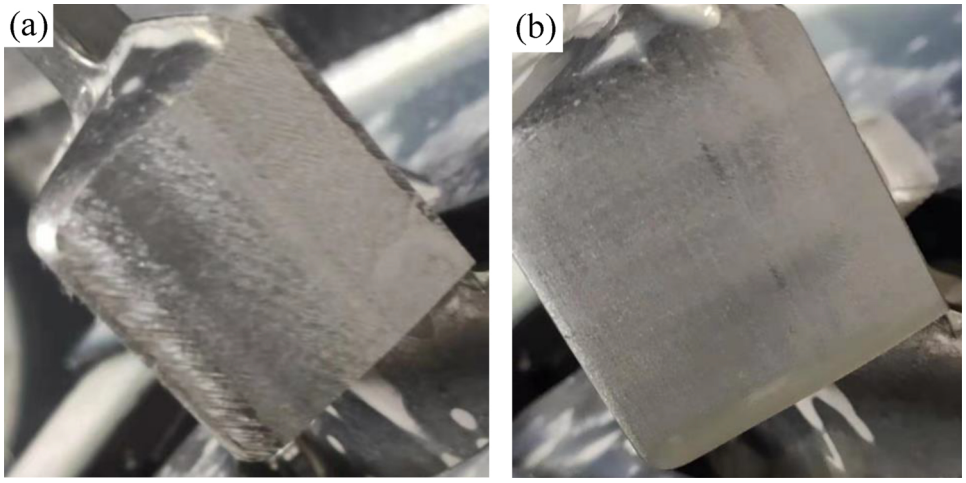

Fig. 24. Surface quality of blade after CNC machining: (a) insufficient fixture stiffness, (b) blade surface quality in the optimized fixture structure.

6. Conclusions

In this work, a technical framework for the design and evaluation of fixture was investigated by algorithm optimization, program development, and experimental analysis. The results can be summarized as follows:

1 The proposed computer-aided fixture design and evaluation system could realize the fixture design and evaluation of the same type blade, and form a systematic fixture design and evaluation method to guide the design, evaluation and manufacture of fixture for near-net-shaped blades.
2 The proposed computer-aided positioning analysis model could analyze the sensitivity of the different component-loops to the closed-loop, and this method of computer-aided positioning analysis could provide guiding significance for the size control of the fixture design. The experimental verification showed that the numerical modeling analysis method was reliable.
3 The established FEM of the blade–fixture system was feasible, and the proposed fixture dynamic analysis method could be used to design and evaluate the fixture. The mechanical modeling analysis of micron-scale manufacturing errors could explain the impact of non-ideal fixture manufacturing errors on the fixture system mechanical behavior. The FEM and the established experimental platform could adequately explain the mechanical behaviors of the blade–fixture system.
4 The proposed computer-aided fixture layout optimization method based on the FEA and genetic algorithm was feasible, and the best fixture layout was obtained by comparative experiments with different fixtures.

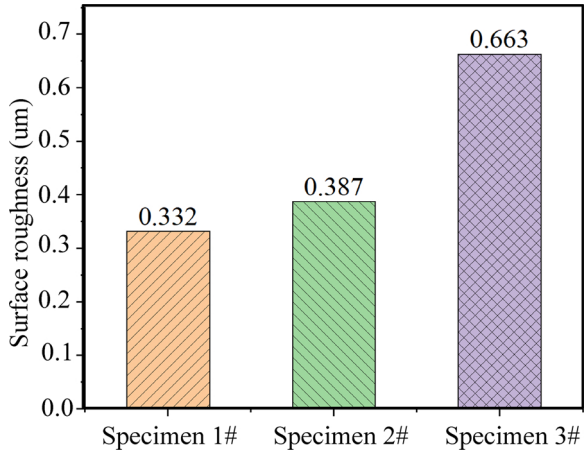

Fig. 25. Surface roughness of different test specimens.

However, the design method of this manuscript is based on the characteristics of statics. It's undeniable that the design based on dynamic structure may be the future development trend, and this will lead to a large amount of calculation time, especially when a large number of samples are generated in combination with genetic algorithms. How to realize the dynamic behavior design method of fixture will be the future research trend.

Declaration of Competing Interest

We declare that we have no financial and personal relationships with other people or organizations that can inappropriately influence our work.

Acknowledgements

The author would like to acknowledge the support and contributions of our colleagues in Xi'an Aero-Engine (Group) Ltd. This research is supported in part by Xi'an Aero-Engine (Group) Ltd, and National Natural Science Foundation of China (Grant 51575310). This work is supported in part by the projects of China Qinghai Provincial Science & Technology Department (No. 2019-ZJ-7097).

References

[1] Lin XJ, Wu DB, Yang BY, Wu G, Shan XF, Xiao QB, et al. Research on the mechanism of milling surface waviness formation in thin-walled blades. Int J Adv Manuf Tech 2017;93:2459–70.
[2] Wang H, Wu BH, Li XQ. Advanced machining technology of new generation commercial aero engine blade. Aeronaut Manuf Technol 2014;20:26–31. [Chinese].
[3] Lin XJ, Wu DB, Shan XF, Wu G, Cui T, Zhang Y, et al. Study on flexible CNC polishing process and surface integrity of blade. J Mech Sci Technol 2018;32(6):2735–46.
[4] Lin XJ, Wang WH. Shan CW Research on the new manufacturing process of aero engine blade. Aeronaut Manuf Technol 2009;45(05):262–74. [Chinese].
[5] Marini D, Cunningham D, Corney JR. Near net shape manufacturing of metal: a review of approaches and their evolutions. P I Mech Eng B J Eng 2018;232(4):650–69. (650–669).
[6] Katz R, Srivatsan V, Patil L. Closed-loop machining cell for turbine blades. Int J Adv Manuf Tech 2011;55(9):869–81.
[7] Wang Hui, (Kevin) Rong Yiming. Case based reasoning method for computer aided welding fixture design. Comput Aided Des 2008;40(12):1121–32. ISSN 0010-4485.
[8] Wang Hui, (Kevin) Rong Yiming, Li Hua. Price Shaun,Computer aided fixture design: recent research and trends. Comput Aided Des 2010;42(12):1085–94. ISSN 0010-4485.
[9] Zhang Z, Zhang D, Luo M, Wu B. Research of machining vibration restraint method

for compressor blade. Procedia CIRP 2016;56:133–6.
[10] Wang H, Wu BH, Li XQ. Advanced machining technology of new generation commercial aero engine blade. Aeronaut Manuf Technol 2014;20:29–30. (in Chinese).
[11] Wu Dongbo, Wang# Hui, Yu Jie, Zhang Kaiyao. Research on machining fixture for adaptive CNC processing technology of near-net-shaped jet engine blade. Chin J Aeronaut 2019. S1000-9361(19)30252-30253.
[12] M E, H S, F F. Influence of fixtures on dimensional accuracy in machining processes. Int J Adv Manuf Technol 2003;21(5):384–90.
[13] Y R, W H, Y K. Locating error analysis and tolerance assignment for computer-aided fixture design. Int J Prod Res 2001;39(15):3529–45.
[14] Hui W, Zhou M, Jie Y, Wang W, Huang B, Rong Y. Numerical modeling and analysis of positioning error in aero-engine blade conformal machining. Comput Integr Manuf Syst 2016;22(09):2118–26.
[15] Hui W, Lijiang H, Chao Y. Integrated analysis method of thin-walled turbine blade precise manufacturing. Int J Precis Eng Manuf 2015;16(5):1011–9.
[16] Katz R, Srivatsan V, Patil L. Closed-loop machining cell for turbine blades. Int J Adv Manuf Technol 2011;55(9-12):869–81.
[17] Hamedi Mohsen. Intelligent fixture design through a hybrid system of artificial neural network and genetic algorithm. Artif Intell Rev 2005;23:295–311.
[18] Wang YQ, Mei ZY, Fan YQ. Finite element optimization of machining fixture layout of thin-walled arc workpiece. Chin J Mech Eng 2005;41(6):214–7.
[19] Qin GH, Wu ZX, Zhang WH. Analysis and control technique of fixturing deformation mechanism of thin-walled workpiece. Chin J Mech Eng 2007;43(4):211–6.
[20] Zhou XL, Zhang WH, Qing GH, et al. On optimizing fixture layout and clamping force simultaneously using genetic algorithm. Mech Sci Technol 2005;24(3):339–42.
[21] Chen WF, Ni LJ, Wang NS. Investigation on optimization method for fixture layout and clamping forces. China Mech Eng 2007;18(12):1413–7.
[22] Zhang KY, Wu DB, Guo XF, et al. High-resolution Tenon distortion test system for blade processing. Mech Sci Technol 2019:04.
[23] Wu Dongbo, Wang# Hui, Peng Jinsong, Zhang Kaiyao, Yu Jie, Li Yuan, et al. Analysis of machining deformation for adaptive CNC machining technology of near-net-Shaped jet engine blade. Int J Adv Manuf Technol 2020. https://doi.org/10.1007/s00170-019-03898-6.
[25] Wang Hui, Liu Tianye, Zhang Zheng, Pei Guoqing, Ye Lang, Xu Xu. Investigation on the precision mounting process of large-aperture Potassium dihydrogen phosphate converters based on accurate prediction model. Precis Eng 2019;57:73–82.